TWO-EQUATION MODEL COMPUTATIONS OF HIGH-SPEED (M_∞=2.25, 7.2), TURBULENT BOUNDARY LAYERS

A Thesis

by

SRIRAM S. ARASANIPALAI

Submitted to the Office of Graduate Studies of
Texas A&M University
in partial fulfillment of the requirements for the degree of

MASTER OF SCIENCE

December 2008

Major Subject: Mechanical Engineering

TWO-EQUATION MODEL COMPUTATIONS OF HIGH-SPEED (M_∞=2.25, 7.2), TURBULENT BOUNDARY LAYERS

A Thesis

by

SRIRAM S. ARASANIPALAI

Submitted to the Office of Graduate Studies of
Texas A&M University
in partial fulfillment of the requirements for the degree of

MASTER OF SCIENCE

Approved by:

Chair of Committee,	Sharath S. Girimaji
Committee Members,	N.K. Anand
	Rodney Bowersox
Head of Department,	Dennis O'Neal

December 2008

Major Subject: Mechanical Engineering

ABSTRACT

Two-equation Model Computations of High-speed (M_∞=2.25, 7.2),
Turbulent Boundary Layers. (December 2008)
Sriram S. Arasanipalai, B.Tech., Indian Institute of Technology, Madras
Chair of Advisory Committee: Dr. Sharath S. Girimaji

The objective of this research is to assess the performance of two popular Reynolds-averaged Navier-Stokes (RANS) models, standard $k-\epsilon$ and $k-\omega$, and to suggest modifications to improve model predictions for high-speed flows. Numerical simulations of turbulent flow past a flat plate are performed at $M_\infty = 2.25, 7.2$. The results from these two Mach number cases are compared with Direct Numerical Simulation (DNS) results from Pirozzoli *et al.* (2004) and experimental results from Horstman & Owen (1975). The effect of the Boussinesq coefficient (C_μ) and turbulent transport coefficients ($\sigma_k, \sigma_\epsilon; \sigma, \sigma^*$) on the boundary layer flow is examined. Further, the performance of a new model with realizability-based correction to C_μ and corresponding modifications to σ, σ^* is examined. The modification to C_μ is based on controlling the ratio of production to dissipation of kinetic energy (P/ϵ). The first choice of $P/\epsilon = 1$ ensures that there is no accumulation of kinetic energy in stagnation or free-stream regions of the flow. The second choice of $P/\epsilon \approx 1.6$ holds under the assumption of a homogeneous shear flow. It is observed that the new model's performance is similar to that of the existing RANS models, which is expected for a simple flow over a flat plate. Finally, the role of turbulent Prandtl number (Pr_t) in temperature and density predictions is established. The results indicate that the $k-\omega$ model's performance is better compared to that of the standard $k-\epsilon$ model for high Mach number flows. A modification to C_μ must be accompanied with corresponding changes to $\sigma_k, \sigma_\epsilon; \sigma, \sigma^*$ for an accurate log-layer prediction. The results also indicate

that a Pr_t variation is required across the boundary layer for improved temperature and density predictions in high-speed flows.

To my family for their love and encouragement

ACKNOWLEDGMENTS

I would like to thank Dr. Sharath Girimaji for believing in me and supporting my education at Texas A&M University. The last two years have been very enjoyable. I would also like to thank Dr. N.K. Anand and Dr. Rodney Bowersox for their participation on my committee and helping me with my master's thesis. I would like to acknowledge Dr. Ravi Srinivasan and Sunil Lakshmipathy for being very patient with me and helping me throughout my research.

I thank all the other members in my research group for their help and support. I also thank the Departments of Mechanical Engineering and Aerospace Engineering for ensuring a smooth sailing through my master's. Last, but not the least, I would like to thank my parents, wife and sister for keeping me motivated all along.

TABLE OF CONTENTS

CHAPTER Page

I INTRODUCTION 1

A Literature survey 1
1 Compressibility effects 2
2 Low-Reynolds-number effects 3
B Present study 4
C Thesis outline 5

II GOVERNING EQUATIONS AND TURBULENCE MODELING 7

A Governing equations 7
B Favre averaging 10
C Favre-averaged Navier-Stokes equations 11
D Turbulence modeling 12
E Two-equation models 13
1 The $k-\epsilon$ model 14
2 The $k-\omega$ model 15
F C_μ variation 18
G Variation of turbulent Prandtl number 22
1 Study 1 23
2 Study 2 24
3 Study 3 24
4 Study 4 24

III NUMERICAL PROCEDURE 26

A $M_\infty = 2.25$ 26
B $M_\infty = 7.2$ 32

IV RESULTS 35

A Study 1: Performance of the standard $k-\epsilon$ and $k-\omega$ turbulence models 35
B Study 2: The effect of turbulent transport coefficients $(\sigma_k, \sigma_\epsilon, \sigma, \sigma^*)$ and the Boussinesq closure coefficient (C_μ) on boundary layer prediction 39

CHAPTER Page

C Study 3: Performance of the new model with realizability-based correction to the Boussinesq coefficient and corresponding modifications to transport coefficients 45
1 M_∞=2.25 45
2 M_∞=7.2 48
D Study 4: The role of turbulent Prandtl number in temperature and density predictions 51

V CONCLUSIONS 58

A Performance of the standard $k-\epsilon$ and $k-\omega$ turbulence models 58
B The effect of turbulent transport coefficients ($\sigma_k, \sigma_\epsilon, \sigma, \sigma^*$) and the Boussinesq closure coefficient (C_μ) on boundary layer prediction 59
C Performance of the new model with realizability-based correction to the Boussinesq coefficient and corresponding modifications to transport coefficients 59
D The role of turbulent Prandtl number in temperature and density predictions 60

REFERENCES 61

VITA 63

LIST OF TABLES

TABLE Page

1 Simulation Boundary Conditions, $M_\infty = 2.25$ 28

2 FLUENT Computational Settings 30

3 Convergence Criteria 30

4 Simulation Boundary Conditions, $M_\infty = 7.2$ 33

5 C_μ Variation Study, $M_\infty = 2.25$ 45

LIST OF FIGURES

FIGURE		Page
1	Computational domain, M_∞= 2.25 case	28
2	Grid adequacy study, M_∞= 2.25 case	31
3	Computational domain, M_∞= 7.2 case	33
4	Grid adequacy study, M_∞= 7.2 case	34
5	Performance of $k-\epsilon$ and $k-\omega$ models: u^+ vs. y^+, $M_\infty = 2.25$ . . .	36
6	Performance of $k-\epsilon$ and $k-\omega$ models: k vs. y, $M_\infty = 2.25$	37
7	Performance of $k-\epsilon$ and $k-\omega$ models: μ_t vs. y, $M_\infty = 2.25$	37
8	Performance of $k-\epsilon$ and $k-\omega$ models: T/T_e vs. y/δ, $M_\infty = 2.25$ . .	38
9	Performance of $k-\epsilon$ and $k-\omega$ models: ρ/ρ_e vs. y/δ, $M_\infty = 2.25$ . .	39
10	Reynolds number effect on $k-\omega$ model mean velocity prediction, $M_\infty = 2.25$	40
11	Effect of Boussinesq coefficient: u^+ vs. y^+, $M_\infty = 2.25$	41
12	Effect of Boussinesq coefficient: k vs. y, $M_\infty = 2.25$	42
13	Effect of Boussinesq coefficient: μ_t vs. y, $M_\infty = 2.25$	42
14	Effect of transport coefficients: u^+ vs. y^+, $M_\infty = 2.25$	43
15	Effect of transport coefficients: k vs. y, $M_\infty = 2.25$	44
16	Effect of transport coefficients: μ_t vs. y, $M_\infty = 2.25$	44
17	Variable β^* model evaluation: u^+ vs. y^+, $M_\infty = 2.25$	46
18	Variable β^* model evaluation: k vs. y, $M_\infty = 2.25$	47

FIGURE Page

19 Variable β^* model evaluation: μ_t vs. y, $M_\infty = 2.25$ 47

20 Variable β^* model evaluation: T/T_e vs. y/δ, $M_\infty = 2.25$ 48

21 Variable β^* model evaluation: ρ/ρ_e vs. y/δ, $M_\infty = 2.25$ 49

22 Variable β^* model evaluation: u^+ vs. y^+, $M_\infty = 7.2$ 49

23 Variable β^* model evaluation: T/T_e vs. y/δ, $M_\infty = 7.2$ 50

24 Variable β^* model evaluation: ρ/ρ_e vs. y/δ, $M_\infty = 7.2$ 50

25 Effect of Pr_t: T/T_e vs. y/δ, $M_\infty = 2.25$ 52

26 Effect of Pr_t: near-wall T/T_e vs. y/δ, $M_\infty = 2.25$ 53

27 Effect of Pr_t: ρ/ρ_e vs. y/δ, $M_\infty = 2.25$ 53

28 Variable Pr_t: T/T_e vs. y/δ, $M_\infty = 2.25$ 54

29 Variable Pr_t wall prediction: T/T_e vs. y/δ, $M_\infty = 2.25$ 55

30 Variable Pr_t: ρ/ρ_e vs. y/δ, $M_\infty = 2.25$ 55

31 Variable Pr_t: T/T_e vs. y/δ, $M_\infty = 7.2$ 56

32 Variable Pr_t: ρ/ρ_e vs. y/δ, $M_\infty = 7.2$ 56

CHAPTER I

INTRODUCTION

Turbulence in fluids comprises of motions over a broad spectrum of scales. An accurate computational procedure must either directly solve for these scales of motion or model them adequately. This multi-scale phenomenon is even more complicated in compressible flows due to the interaction between thermodynamic (density, temperature) and flow variables (pressure and velocity). One of the key compressible flow phenomenon of aerodynamic interest is the shock-boundary layer interaction (Thivet, 2002). This interaction can lead to boundary layer separation and subsequent reattachment. In internal flow applications, compressible turbulence plays a key role in fuel-air mixing and reaction. Accurate mixing prediction is impossible unless the underlying velocity field description is adequately modeled. The subject of this thesis is the modeling of compressible flows.

A Literature survey

Over the last fifty years a wide variety of incompressible turbulence models, based on the Reynolds-Averaged Navier-Stokes (RANS) equations, have been developed at various levels of approximation. The use of these turbulence models significantly reduce the required computational resources in comparison to Direct Numerical Simulations (DNS). On the other hand, relatively less progress has been made in the compressible regime primarily due to intrinsic difficulties, both in experiments and numerical simulations. While DNS has become a powerful tool over the past two decades, most studies were restricted to low Reynolds number cases and simple geometries to reduce

---

The journal model is *Journal of Fluid Mechanics*.

computational demands.

Among the incompressible turbulence models, the two-equation models are widely used in engineering applications. Hence, it is important to test the performance of the existing two-equation turbulence models for compressible flows in order to develop modifications to improve their flow predictions. Furthermore, the same length scale equation (either ϵ or ω) can be used in higher order closures such as the seven-equation Reynolds stress closure methods.

1 Compressibility effects

Incompressible models for Reynolds stress, heat-flux, diffusion and transport can be extended to compressible flows with suitable modifications (Wilcox, 1994). The presence of density and temperature variations in compressible flows lead to several terms not present in the averaged governing equations for incompressible flows: pressure-dilatational correlation tensor, pressure-dilatation and dilatational dissipation (Wilcox, 1994). Currently, for these terms, closure models of Sarkar *et al.* (1989) and Zeman (1990) are most widely used. A modification to these closure models was proposed by Wilcox (1992). Most compressibility effects in these closure models manifest through dilatational dissipation. However, as Sarkar points out, most of the difference in the physics of incompressible and compressible flows is due to pressure effects. Therefore, improved compressibility correction models are needed.

Using a near-wall mixing length theory (which accounts for density variations) and the Crocco-Busemannn approximation (Wilcox, 1994), van Driest obtained a closed form expression for mean velocity along the flow direction as a function of wall-normal distance. The use of van Driest effective velocity (Wilcox, 1994) correlates compressible, near-wall flows with the incompressible law of the wall. Wilcox

(1994) states that both $k-\epsilon$ and $k-\omega$ turbulence models provide reasonably accurate log-layer predictions for constant-pressure, adiabatic-wall boundary layers for Mach number upto 5. However, the performance of the $k-\epsilon$ model for adverse pressure gradient compressible flows is not as good as that of the $k-\omega$ model. The presence of a non-physical density effect affects the log-layer prediction of $k-\epsilon$ model for simple boundary layer flows and adverse pressure gradient flows at high mach numbers. However, in the $k-\omega$ model this non-physical density profile is not as pronounced as in the $k-\epsilon$ model.

2 Low-Reynolds-number effects

The standard $k-\epsilon$ model and the $k-\omega$ model are restricted to high Reynolds number applications. For example, these models fail to predict the sharp peak in turbulent kinetic energy, k, close to the surface for channel flows. Also, most two equation models fail to predict a realistic value of the additive constant in the law of the wall (Wilcox, 1994). All these models require viscous damping in order to achieve a realistic value for this additive constant. Several modifications to the existing two-equation models have been developed to address the low-Reynolds-number-effects. Some of the commonly used low-Reynolds-number-corrections are: Jones-Launder model, Launder-Sharma model and Chien Model (Wilcox, 1994).

The commonly used two-equation models give physically realizable (Reynolds normal stresses are non-negative) stresses for simple boundary layer flows (both incompressible and compressible flows) (Durbin, 1996). However, for a flow approaching the leading edge of a body or impinging on a flat plate, non-realizable stresses are predicted and these erroneous stresses cause severe over-production of turbulent kinetic energy (k). In addition, the presence of a shock wave near the stagnation point in high-speed flows further deteriorates the model performance (Sinha *et al.*, 2003).

A suitable correction is needed for the two-equation models to overcome this inherent model deficiency. Such a correction can also improve behavior in low-Reynolds number regions of the flow.

Several realizable turbulence models have been developed over the last two decades for incompressible flows (Durbin, 1996; Moore & Moore, 1999; Shih *et al.*, 1995). These models show significant improvement in turbulent boundary layer predictions downstream of stagnation point. Other type of low-Reynolds number corrections (Jones-Launder model, Launder-Sharma model and Chien Model (Wilcox, 1994)) also yield reasonable results in the stagnation point flows. However, these low-Reynolds number corrections tend to be *ad hoc* and may involve distance-to-the-wall as a parameter in the closure expression. This type of model correction is undesirable as the distance-to-the-wall is not straight forward to compute, 3D and corner flows.

B Present study

This thesis addresses some important unresolved two-equation modeling issues pertaining to high-speed turbulent boundary layers. The various studies undertaken are:

1. Evaluation of the performance of the existing standard $k-\epsilon$ and $k-\omega$ turbulence models in Mach 2.25 boundary layer.

2. Analysis of the effect of turbulent transport coefficients ($\sigma_k, \sigma_\epsilon, \sigma, \sigma^*$) and the Boussinesq closure coefficient (C_μ) on boundary layer prediction.

3. Examination of the performance of a new model with realizability-based correction to the Boussinesq coefficient and corresponding modifications to transport coefficients (Lakshmipathy, 2008).

4. Establishment of the role of turbulent Prandtl number in temperature and density predictions.

Two-dimensional, high-speed (M_∞ =2.25, 7.2), turbulent boundary layer simulations for a flow over a flat plate are performed using FLUENT, a commercial CFD software. Both $k-\epsilon$ and $k-\omega$ closures are investigated. The objective of this study is to assess the performance of these models for high speed flows by comparing against the available experimental/DNS data: Pirozzoli *et al.* (2004) for $M_\infty = 2.25$ and Horstman & Owen (1975) for $M_\infty = 7.2$. Specifically, the effect of various closure coefficients (C_μ, σ_ϵ, σ_k for $k-\epsilon$ model and β^*, σ, σ^* for $k-\omega$ model) on the compressible boundary layer is studied.

Realizability considerations only yield an inequality and not a specific value for C_μ. In recent work within our research group (Lakshmipathy, 2008) it was suggested that the choice of C_μ should be such that the production to dissipation of kinetic energy ratio is unity ($P/\epsilon \approx 1$) in the stagnation region. This choice of $P = \epsilon$ ensures that there is no accumulation of kinetic energy in stagnation or free-stream regions of the flow. Further, in the equilibrium log-law region, P/ϵ is known to be unity. In production-dominated fully turbulent regions and turbulence decay regions, C_μ assumes its standard value of 0.09.

C Thesis outline

Chapter II first presents the governing equations for compressible fluid flow. Then the Favre-averaged Navier-Stokes equations are derived followed by the presentation of the turbulence models used in FLUENT to close these averaged equations. Finally, the variable C_μ model is developed and corresponding variations in other transport coefficients are described in detail. Chapter III presents the computational setups used

for this study. The results from various issues considered in this study are presented in Chapter IV. Conclusions and recommendations for future work are presented in Chapter V.

CHAPTER II

GOVERNING EQUATIONS AND TURBULENCE MODELING

The governing equations for compressible fluid flow are first presented in this chapter and the Favre-averaged conservation equations are derived from these equations. Then the two widely used two-equation turbulence models: $k-\epsilon$ and $k-\omega$ models are presented. Finally, the variations in Boussinesq closure coefficient and turbulence transport coefficients considered in this study are presented.

A Governing equations

For fluid flow in a compressible medium one must solve the equations governing conservation of mass, momentum and energy. The instantaneous Navier-Stokes equations in tensor notation (Wilcox, 1994) are defined below.

Conservation of mass:

$$\frac{\partial \rho}{\partial t} + \frac{\partial}{\partial x_j}\left(\rho u_j\right) = 0 \tag{2.1}$$

Conservation of momentum:

$$\frac{\partial}{\partial t}\left(\rho u_i\right) + \frac{\partial}{\partial x_j}\left(\rho u_j u_i\right) = -\frac{\partial p}{\partial x_i} + \frac{\partial t_{ji}}{\partial x_j} \tag{2.2}$$

Conservation of energy:

$$\frac{\partial}{\partial t}\left[\rho\left(e + \frac{1}{2}u_i u_i\right)\right] + \frac{\partial}{\partial x_j}\left[\rho u_j\left(h + \frac{1}{2}u_i u_i\right)\right] = \frac{\partial}{\partial x_j}\left(u_i t_{ij}\right) - \frac{\partial q_j}{\partial x_j} \tag{2.3}$$

In the equations shown above, ρ is the density of the fluid, u_i is the ith component of velocity, x_i is the ith component of a position vector in an inertial reference frame and p is the pressure. The specific internal energy is given by e and $h = e + p/\rho$ is the specific enthalpy. In order to solve the equations for compressible flows an equation of state must be specified. The perfect gas law relates the fluid pressure (p), density (ρ) and temperature (T),as follows:

$$p = \rho RT \tag{2.4}$$

where R is the perfect gas constant. Now constitutive relations for the viscous stress tensor t_{ij} and the heat-flux vector q_j are required. For compressible flows, the viscous stress tensor involves both the molecular viscosity, μ and the second viscosity, ζ,

$$t_{ij} = 2\mu s_{ij} + \zeta \frac{\partial u_k}{\partial x_k} \delta_{ij} \tag{2.5}$$

where s_{ij} is the instantaneous strain-rate tensor,

$$s_{ij} = \frac{1}{2}\left(\frac{\partial u_i}{\partial x_j} + \frac{\partial u_j}{\partial x_i}\right) \tag{2.6}$$

and δ_{ij} is the Kronecker delta,

$$\delta_{ij} = \begin{cases} 1 & \text{if } i = j \\ 0 & \text{if } i \neq j \end{cases} \tag{2.7}$$

The heat-flux vector is obtained from Fourier's law as:

$$q_j = -\kappa \frac{\partial T}{\partial x_j} \tag{2.8}$$

where κ represents the thermal conductivity.

The above system of equations can be simplified by making two assumptions. The first relates second viscosity to the molecular viscosity.

$$\zeta = -\frac{2}{3}\mu \tag{2.9}$$

This assumption holds true for monatomic gases and is generally used for all gases in engineering applications (Wilcox, 1994). Secondly it is assumed that the gas is calorically perfect i.e. the specific heat coefficients for constant volume, C_v, and constant pressure, C_p, processes are themselves constant and independent of temperature. Hence,

$$e = C_v T \quad h = C_p T \tag{2.10}$$

These relations lead to

$$q_j = -\kappa \frac{\partial T}{\partial x_j} = -\frac{\mu}{Pr_L} \frac{\partial h}{\partial x_j} \tag{2.11}$$

where

$$Pr_L = \frac{C_p \mu}{\kappa} \tag{2.12}$$

Here Pr_L is the Prandtl number.

B Favre averaging

For a compressible flow, the density and temperature fluctuations must be accounted for in addition to velocity and pressure fluctuations resulting from turbulent motion. Furthermore, the Reynolds averaging procedure gives rise to additional terms in the mean conservation equations; these new terms have no analogs in the laminar flow equations and increase the difficulty in establishing closure approximations Wilcox (1994). In order to overcome this difficulty, Favre (1965) suggested a density-weighted averaging procedure, in which a *mass averaged* velocity, $\widetilde{u}_i$, is defined as follows:

$$\widetilde{u}_i = \frac{1}{\overline{\rho}} \lim_{T\to\infty} \int_t^{t+T} \rho\left(X,\tau\right) u_i\left(X,\tau\right) d\tau \tag{2.13}$$

Here $\overline{\rho}$ is the Reynolds-averaged density. This implies that:

$$\overline{\rho}\widetilde{u}_i = \overline{\rho u_i} \tag{2.14}$$

The instantaneous velocity, u_i, is then decomposed into a mass-averaged part and a fluctuating part, u_i'' as shown:

$$u_i = \widetilde{u}_i + u_i'' \tag{2.15}$$

Multiplying (2.15) by ρ and performing a Reynolds average yields

$$\overline{\rho u_i} = \overline{\rho}\widetilde{u}_i + \overline{\rho u_i''} \tag{2.16}$$

Using (2.14) it can be shown that

$$\overline{\rho u_i''} = 0 \tag{2.17}$$

It should be noted that Favre averaging is only a convenient way of handling the mean and fluctuating quantities in a compressible flow. It is not a physical simplification (Wilcox, 1994).

C Favre-averaged Navier-Stokes equations

To perform Favre-average of the conservation equations (2.1, 2.2 and 2.3), the flow properties are decomposed as follows:

$$u_i = \widetilde{u}_i + u_i'' \tag{2.18a}$$

$$\rho = \overline{\rho} + \rho' \tag{2.18b}$$

$$p = \overline{p} + p' \tag{2.18c}$$

$$h = \widetilde{h} + h'' \tag{2.18d}$$

$$q_j = \overline{q_{L_j}} + q_j' \tag{2.18e}$$

The instantaneous velocity, enthalpy, internal energy and temperature are decomposed as a mass-averaged part and a fluctuating part. Pressure, density and heat-flux are decomposed by the conventional Reynolds averaging. Using the above relations in the conservation equations (2.1, 2.2 and 2.3) and performing the mass-averaging operations, we arrive at Favre-averaged Navier-Stokes equations.

$$\frac{\partial \overline{\rho}}{\partial t} + \frac{\partial}{\partial x_i}\left(\overline{\rho}\widetilde{u}_i\right) = 0 \tag{2.19}$$

$$\frac{\partial}{\partial t}\left(\overline{\rho}\widetilde{u_i}\right)+\frac{\partial}{\partial x_j}\left(\overline{\rho}\widetilde{u_j}\widetilde{u_i}\right)=-\frac{\partial\overline{p}}{\partial x_i}+\frac{\partial}{\partial x_j}\left[\mu\left(\frac{\partial\widetilde{u_i}}{\partial x_j}+\frac{\partial\widetilde{u_j}}{\partial x_i}-\frac{2}{3}\delta_{ij}\frac{\partial\widetilde{u_k}}{\partial x_k}\right)-\overline{\rho u_j'' u_i''}\right] \quad (2.20)$$

$$\frac{\partial}{\partial t}\left(\overline{\rho}E\right)+\frac{\partial}{\partial x_j}\left(\overline{\rho}\widetilde{u_j}H\right)=\frac{\partial}{\partial x_j}\left[-\overline{q_{L_j}}-\overline{q_{T_j}}+\widetilde{u_i}\left(\widetilde{\tau_{ij}}\right)_{eff}\right] \quad (2.21)$$

$$\overline{p}=\overline{\rho}R\widetilde{T} \quad (2.22)$$

$$E=\widetilde{e}+\frac{1}{2}\widetilde{u_i}\widetilde{u_i}+k \quad (2.23a)$$

$$H=\widetilde{h}+\frac{1}{2}\widetilde{u_i}\widetilde{u_i}+k \quad (2.23b)$$

$$\left(\widetilde{\tau_{ij}}\right)_{eff}=\mu_{eff}\left(\frac{\partial\widetilde{u_j}}{\partial x_i}+\frac{\partial\widetilde{u_j}}{\partial x_i}\right)-\frac{2}{3}\mu_{eff}\frac{\partial\widetilde{u_k}}{\partial x_k}\delta_{ij} \quad (2.23c)$$

In the above system of equations, $\overline{q_{T_j}}$ represents the turbulent heat flux, E is the total internal energy, H is the total enthalpy, $\left(\widetilde{\tau_{ij}}\right)_{eff}$ represents the deviatoric stress and μ_{eff} represents the sum of molecular viscosity, μ, and turbulent viscosity, μ_T.

D Turbulence modeling

The Boussinesq assumption is used to model the new stress term in (2.20) that arises out of Favre averaging.

$$-\overline{\rho u_j'' u_i''}=\mu_t\left(\frac{\partial\widetilde{u_i}}{\partial x_j}+\frac{\partial\widetilde{u_j}}{\partial x_i}\right)-\frac{2}{3}\left(\overline{\rho}k+\mu_t\frac{\partial\widetilde{u_k}}{\partial x_k}\right)\delta_{ij} \quad (2.24)$$

This assumption is used in most of the popular two-equation models like $k-\epsilon$ and $k-\omega$ turbulence models. Additional transport equations are solved to obtain the

value of the turbulent viscosity, μ_t. Modeling for the deviatoric stress, $(\widetilde{\tau_{ij}})_{eff}$ is given in (2.23c).

The turbulent heat-flux vector, $\overline{q_{T_j}}$, which again arises out of averaging, is modeled on the lines of Fourier's law as follows:

$$\overline{q_{T_j}} = \overline{\rho u_j'' h''} = -\frac{\mu_T C_p}{Pr_T}\frac{\partial \widetilde{T}}{\partial x_j} = -\frac{\mu_T}{Pr_T}\frac{\partial \widetilde{h}}{\partial x_j} \tag{2.25}$$

where Pr_T is the turbulent Prandtl number. Usually, a constant value of 0.85 is assumed for Pr_T in engineering applications (Fluent, 2006).The literature reveals that the value of Pr_T in the boundary layer is around 0.9 and for free-shear flows its around 0.5 (Rotta, 1960). So by varying the value Pr_T across a boundary layer, heat transfer predictions can be improved.

E Two-equation models

Two-equation models are one of the simplest complete models of turbulence (Wilcox, 1994). These models served as the foundation for the majority of turbulence model research over the last few decades. These turbulence models usually involve two other transport equations in addition to the averaged conservation equations (equations 2.16-2.20). One of the equations is a transport equation for the turbulent kinetic energy (k) and the other can be a transport equation for dissipation rate (ϵ), specific dissipation rate (ω), length scale (L) or a time scale (τ). Now we present the various two-equation models used in this study. The equations shown are in the notation used in the FLUENT manual (Fluent, 2006).

1 The $k-\epsilon$ model

This is a semi-empirical model and is based on the transport equations for turbulent kinetic energy, k, and dissipation rate, ϵ.

$$\frac{\partial}{\partial t}\left(\overline{\rho}k\right)+\frac{\partial}{\partial x_j}\left(\overline{\rho}k\widetilde{u_j}\right)=\frac{\partial}{\partial x_j}\left[\left(\mu+\frac{\mu_t}{\sigma_k}\right)\frac{\partial k}{\partial x_j}\right]+G_k-\overline{\rho}\epsilon-Y_M \tag{2.26}$$

$$\frac{\partial}{\partial t}\left(\overline{\rho}\epsilon\right)+\frac{\partial}{\partial x_j}\left(\overline{\rho}\epsilon\widetilde{u_j}\right)=\frac{\partial}{\partial x_j}\left[\left(\mu+\frac{\mu_t}{\sigma_\epsilon}\right)\frac{\partial \epsilon}{\partial x_j}\right]+C_{1\epsilon}\frac{\epsilon}{k}G_k-C_{2\epsilon}\overline{\rho}\frac{\epsilon^2}{k} \tag{2.27}$$

The turbulent viscosity is computed as follows:

$$\mu_t=\overline{\rho}C_\mu\frac{k^2}{\epsilon} \tag{2.28}$$

The model constants appearing in (2.26)-(2.28) are given the standard values

$$C_{1\epsilon}=1.44,\ C_{2\epsilon}=1.92,\ C_\mu=0.09,\ \sigma_k=1,\ \sigma_\epsilon=1.3 \tag{2.29}$$

σ_k and σ_ϵ are turbulent Prandtl numbers for k and ϵ respectively. In (2.26), G_k represents the modeled production of turbulent kinetic energy. To be consistent with the Boussinesq assumption G_k is defined as

$$G_k=\mu_t S^2 \tag{2.30a}$$

$$S\equiv\sqrt{2S_{ij}S_{ij}} \tag{2.30b}$$

$$S_{ij} = \frac{1}{2}\left(\frac{\partial \widetilde{u}_i}{\partial x_j} + \frac{\partial \widetilde{u}_j}{\partial x_i}\right) \tag{2.30c}$$

The dilatational dissipation term, Y_M, in (2.26) is included in the k transport equation for high Mach number flows. This term is modeled according to a proposal by Sarkar,

$$Y_M = 2\overline{\rho}\epsilon M_t^2 \tag{2.31a}$$

$$M_t = \sqrt{\frac{k}{a^2}} \tag{2.31b}$$

where M_t is the turbulent Mach number and a is the speed of sound.

2 The $k-\omega$ model

The $k-\omega$ model in FLUENT is based on Wilcox's $k-\omega$ model that incorporates modifications for low-Reynolds number effect, compressibility and shear flow spreading. This model is again an empirical model based on model transport equations for turbulent kinetic energy k and specific dissipation rate, ω (ratio of ϵ to k) (Wilcox, 1994).

$$\frac{\partial}{\partial t}(\overline{\rho}k) + \frac{\partial}{\partial x_j}(\overline{\rho}k\widetilde{u_j}) = \frac{\partial}{\partial x_j}\left(\Gamma_k \frac{\partial k}{\partial x_j}\right) + G_k - Y_k \tag{2.32}$$

$$\frac{\partial}{\partial t}(\overline{\rho}\omega) + \frac{\partial}{\partial x_j}(\overline{\rho}\omega\widetilde{u_j}) = \frac{\partial}{\partial x_j}\left(\Gamma_\omega \frac{\partial \omega}{\partial x_j}\right) + G_\omega - Y_\omega \tag{2.33}$$

where G_k is as defined in (2.30a) and G_ω represents the production of ω. Γ_k and Γ_ω represent the effective diffusivity of k and ω respectively. Y_k and Y_ω represent the dissipation of k and ω due to turbulence.

The effective diffusivitites for the $k-\omega$ model are defined as:

$$\Gamma_k = \mu + \frac{\mu_t}{\sigma_k} \tag{2.34a}$$

$$\Gamma_\omega = \mu + \frac{\mu_t}{\sigma_\omega} \tag{2.34b}$$

where $\sigma_k = 2.0$ and $\sigma_\omega = 2.0$ are turbulent Prandtl numbers for k and ω respectively. In this model the turbulent viscosity is given by

$$\mu_t = \alpha^* \frac{\overline{\rho} k}{\omega} \tag{2.35}$$

where

$$\alpha^* = \alpha^*_\infty \left(\frac{\alpha^*_0 + Re_t/R_k}{1 + Re_t/R_k} \right) \tag{2.36a}$$

$$Re_t = \frac{\rho k}{\mu \omega} \tag{2.36b}$$

$$R_k = 6 \tag{2.36c}$$

$$\alpha^*_0 = \beta_i/3 \tag{2.36d}$$

$$\beta_i = 0.072 \tag{2.36e}$$

The above definitions are for a low-Reynolds number flow and for high-Reynolds-number flow, $\alpha^* = \alpha^*_\infty = 1$ (Fluent, 2006).

The production of turbulent kinetic energy G_k is defined in the same way as in (2.30a) and the production of ω is given by

$$G_\omega = \alpha \frac{\omega}{k} G_k \tag{2.37}$$

The coefficient α is given by

$$\alpha = \frac{\alpha_\infty}{\alpha^*}\left(\frac{\alpha_0^* + Re_t/R_\omega}{1 + Re_t/R_\omega}\right) \tag{2.38a}$$

$$R_\omega = 2.95 \tag{2.38b}$$

α^* and Re_t are given by (2.36a) and (2.36b) respectively. Again, for high-Reynolds-number flow, $\alpha^* = \alpha_\infty^* = 1$ (Fluent, 2006).

The dissipation of k, Y_k, is given by

$$Y_k = \rho\beta^* f_{\beta^*} k\omega \tag{2.39a}$$

$$f_{\beta^*} = \begin{cases} 1 & \text{if } \chi_k \leq 0 \\ \frac{1+680\chi_k^2}{1+400\chi_k^2} & \text{if } \chi_k > 0 \end{cases} \tag{2.39b}$$

$$\chi_k = \frac{1}{\omega^3}\frac{\partial k}{\partial x_j}\frac{\partial \omega}{\partial x_j} \tag{2.39c}$$

$$\beta^* = \beta_i^*\left[1 + \zeta^* F(M_t)\right] \tag{2.39d}$$

$$\beta_i^* = \beta_\infty^*\left(\frac{4/15 + (Re_t/R_\beta)^4}{1 + (Re_t/R_\beta)^4}\right) \tag{2.39e}$$

$$\zeta^* = 1.5 \tag{2.39f}$$

$$R_\beta = 8 \tag{2.39g}$$

$$\beta_\infty^* = 0.09 \tag{2.39h}$$

where Re_t is given by Equation (2.36b).

$$Y_\omega = \rho\beta f_\beta \omega^2 \tag{2.40a}$$

$$f_\beta = \frac{1 + 70\chi_\omega}{1 + 80\chi_\omega} \tag{2.40b}$$

$$\chi_\omega = \left| \frac{\Omega_{ij}\Omega_{ij}S_{ki}}{(\beta^*_\infty \omega)^3} \right| \tag{2.40c}$$

$$\Omega_{ij} = \frac{1}{2}\left(\frac{\partial \widetilde{u_i}}{x_j} - \frac{\partial \widetilde{u_j}}{x_i} \right) \tag{2.40d}$$

S_{ij} is as defined in (2.30c) and

$$\beta = \beta_i \left[1 - \frac{\beta^*_i}{\beta_i} \zeta^* F(M_t) \right] \tag{2.41}$$

where β^*_i is defined in (2.39d) and $F(M_t)$ is defined below.

The compressibility correction, $F(M_t)$, used in this model when solving for compressible flows is presented below.

$$F(M_t) = \begin{cases} 0 & \text{if } M_t \leq M_{t0} \\ M_t^2 - M_{t0}^2 & \text{if } M_t \geq M_{t0} \end{cases} \tag{2.42}$$

where M_t and a are as defined in (2.31b) and $M_{t0} = 0.25$. For high-Reynolds-number flow, $\beta^*_i = \beta^*_\infty$, where β^*_i is defined in (2.39d) and $\beta^*_\infty = 0.09$.

F C_μ variation

Realizability is a requirement that each of the Reynolds normal stresses be non-negative and bounded by $2k$ (Moore & Moore, 1999). The two-equation models predict physically realizable stresses for simple boundary layer flows but can predict non-realizable stresses for a flow approaching the leading edge of a body or a flow impinging on a flat plate (Durbin, 1996; Moore & Moore, 1999; Shih *et al.*, 1995). For supersonic flows, the error in the prediction of the Reynolds stresses is further

magnified by the presence of a shock wave near the stagnation point (Sinha *et al.*, 2003).

For the $k-\epsilon$ model, the eddy viscosity is given by

$$\nu_t = C_\mu k^2/\epsilon \tag{2.43}$$

with a constant C_μ value of 0.09. The Reynolds stresses for an incompressible flow are given by

$$\overline{u_i u_j}/k = -2C_\mu \left(k/\epsilon\right) S_{ij} + \frac{2}{3}\delta_{ij} \tag{2.44}$$

where $\overline{u_i}$ is the fluctuating component of the velocity and S_{ij} is the mean strain rate tensor. It can be seen that the $k-\epsilon$ model will yield a non-realizable value of $\overline{u_i u_j}$ when $S_{11}k/\epsilon$ is greater than 3.7. A negative value of the Reynolds normal stress leads to the over-production of turbulent kinetic energy (Durbin, 1996; Moore & Moore, 1999). In order to have a realizable two-equation model, the value of C_μ cannot be a constant.

Several realizable two-equation models with variable C_μ have been proposed (Durbin, 1996; Moore & Moore, 1999; Reynolds, 1987; Shih *et al.*, 1995). In this study a new realizable, variable C_μ model is proposed. The variation in C_μ is designed to yield ratio of production to dissipation of turbulent kinetic energy ($G_k/\overline{\rho}\epsilon$) of unity which is reasonable in an equilibrium boundary layer. This also prevents unphysical growth of turbulent kinetic energy in the stagnation point region.

For the sake of simplicity, the development of the variable C_μ model is shown for a two-dimensional incompressible flow. However, the model is equally applicable to compressible flows. The model development begins with the assumption that the

production of turbulent kinetic energy equals dissipation of turbulent kinetic energy,

$$\mu_t S^2 = \overline{\rho}\epsilon \tag{2.45}$$

where S is the strain rate magnitude (2.30b). Using (2.28), the variation in C_μ is obtained as

$$C_\mu = \left(\frac{\epsilon}{Sk}\right)^2 \tag{2.46}$$

The above variation in C_μ must satisfy the realizability constraint. To show this, it is enough to prove that each of the Reynolds normal stresses is non-negative (Durbin, 1996). In the principal coordinate frame, the Reynolds normal stresses are given by

$$\frac{\overline{u_\alpha^2}}{k} = -2C_\mu \frac{k}{\epsilon}\lambda_\alpha + \frac{2}{3} \tag{2.47}$$

where λ_α (for $\alpha = 1, 2$) are the eigenvalues of the strain rate tensor S_{ij} and

$$\lambda_1^2 + \lambda_2^2 = S^2 \tag{2.48a}$$

$$\lambda_1 + \lambda_2 = 0 \tag{2.48b}$$

for a two-dimensional incompressible flow. It follows from (2.48a) and (2.48b) that

$$|\lambda_\alpha| = \sqrt{S^2/2} \tag{2.49}$$

Using (2.46), (2.47) and (2.49), the realizability constraint, $\overline{u_\alpha^2} \geq 0$, takes the form

$$-\frac{\epsilon}{Sk} + \frac{\sqrt{2}}{3} \geq 0 \tag{2.50}$$

The variable C_μ model is used in computations only when $(\epsilon/Sk)^2$ is less than 0.09 or in other words, when (ϵ/Sk) is less than 0.3. For these values of (ϵ/Sk) the realizability constraint (2.50) is always satisfied. Like the Durbin's model (Durbin, 1996), the variable C_μ model developed in this work can be implemented computationally as follows:

$$C_\mu = \min\left[\left(\frac{\epsilon}{Sk}\right)^2, 0.09\right] \tag{2.51}$$

By solving the x-momentum equation and the turbulence transport equations in the log-layer region (Wilcox, 1994), the relationships among the various model coefficients are obtained as

$$\kappa^2 = \sqrt{C_\mu}\,(C_{\epsilon 2} - C_{\epsilon 1})\,\sigma_\epsilon \tag{2.52a}$$

$$\kappa^2 = \sqrt{\beta^*}\,(\beta/\beta^* - \alpha)\,\sigma_\omega \tag{2.52b}$$

for $k-\epsilon$ and $k-\omega$ models, respectively. Here $\kappa = 0.41$ is the von Karman constant, $C_{\epsilon 1}$, $C_{\epsilon 2}$ and α, β are model constants. The coefficient β^* in the $k-\omega$ model is the equivalent of C_μ in the $k-\epsilon$ model.

A variation in C_μ or β^* alone, would violate (2.52a) and (2.52b) and affect the behavior in the log-layer region of a turbulent boundary layer. To obtain the correct behavior, the model transport coefficients (σ_ϵ for $k-\omega$ model and σ_ω for $k-\omega$ model) are modified based on (2.52a) and (2.52b). For a given C_μ or β^* variation,

the corresponding variations for these model transport coefficients (σ_ϵ, σ_ω) can be obtained from (2.52a) and (2.52b).

The other model transport coefficient, σ_k, can be varied independently. The variation considered in this study is based on

$$\left(\frac{\sigma_\epsilon}{\sigma_k}\right)_{C_\mu=0.09} = \left(\frac{\sigma_\epsilon}{\sigma_k}\right)_{C_\mu variable} \tag{2.53a}$$

$$\left(\frac{\sigma_\omega}{\sigma_k}\right)_{C_\mu=0.09} = \left(\frac{\sigma_\omega}{\sigma_k}\right)_{C_\mu variable} \tag{2.53b}$$

for $k-\epsilon$ and $k-\omega$ models, respectively.

G Variation of turbulent Prandtl number

The turbulent heat-flux vector ($\overline{q_{T_j}}$), which arises out of Favre-averaging of energy conservation equation (Wilcox, 1994), is modeled as

$$\overline{q_{T_j}} = -\overline{\rho u_j'' h''} = -\frac{\mu_T C_p}{Pr_T}\frac{\partial \widetilde{T}}{\partial x_j} = -\frac{\mu_T}{Pr_T}\frac{\partial \widetilde{h}}{\partial x_j}$$

where ρ is the density, h'' is the fluctuating component of specific enthalpy, u_j'' is the fluctuating component of the velocity, μ_T is the turbulent viscosity, C_p is the specific heat at constant pressure, Pr_T is the turbulent Prandtl number and $\widetilde{T}$ is the Favre-averaged temperature.

Usually, a constant value of 0.85 is assumed for Pr_T in engineering applications. In reality, the value of Pr_T varies across the boundary layer. A variation in Pr_T proposed by Rotta (Rotta, 1960) is used in this study, and its effect on temperature prediction is examined.

$$Pr_T = 0.9 - 0.4\left(\frac{y}{\delta}\right)^2 \tag{2.54}$$

Here, δ is the boundary layer thickness.

In this thesis, several studies are performed to assess current model behavior and examine the new realizability-based model for compressible flows. The various studies are:

1. Study 1: Performance of the standard $k-\epsilon$ and $k-\omega$ turbulence models.

2. Study 2: The effect of turbulent transport coefficients ($\sigma_k, \sigma_\epsilon, \sigma, \sigma^*$) and the Boussinesq closure coefficient (C_μ) on boundary layer prediction.

3. Study 3: Performance of the new model with realizability-based correction to the Boussinesq coefficient and corresponding modifications to transport coefficients.

4. Study 4: The role of turbulent Prandtl number in temperature and density predictions.

1 Study 1

The objective of this study is to assess the performance of two popular Reynolds-averaged Navier-Stokes (RANS) based turbulence models: standard $k-\epsilon$ and $k-\omega$ turbulence models, in a Mach 2.25 boundary layer. The mean flow and turbulence quantities are compared with the available data (Pirozzoli *et al.*, 2004).

In addition, the Reynolds number effect on $k-w$ model's flow predictions is examined by analysing the results at the oulet of the computational domain (figure 1).

2 Study 2

Tandra *et al.* (2006) suggested a new realizability-based $k-\epsilon$ model for supersonic jet flows. A correction to C_μ was proposed and the transport coefficients σ_ϵ and σ_k were unaltered. In this study, the effect of variation in β^* alone on the boundary layer performance is first examined. Then the transport coefficients are changed on the lines of 2.52b and 4.1, respectively and the effect of these changes on the boundary layer prediction is studied.

3 Study 3

The new realizability-based model (Lakshmipathy, 2008) has been tested for incompressible stagnation point flows and adverse pressure gradient flows. Significant improvement in the flow predictions, especially the turbulent kinetic energy predictions, has been observed. The purpose of this study is to assess the new model's performance for compressible flows over a flat plate at different Mach numbers (2.25 and 7.2).Realizability-based variation to β^* (2.46) and corresponding variations in σ_ω and σ_k (2.52b and 4.1) are used. The new model's performance is compared against that of the standard $k-\omega$ model.

4 Study 4

The current RANS two-equation models assume a constant value of 0.85 for turbulent Prandtl number, Pr_t (Wilcox, 1994). However, in the DNS and the experimental studies (Pirozzoli *et al.*, 2004; Horstman & Owen, 1975), it was shown that the value of Pr_t is not a constant across a boundary layer. The value of Pr_t is about 1 close to the wall and about 0.5 at the free-stream. The Pr_t variation proposed by Rotta (2.54) fits the DNS and experimental observations. Hence, in this study, (2.54) is

used to examine the effect of Pr_t variation on temperature and density predictions. This study is performed at two different free-stream Mach numbers: 2.25 and 7.2.

CHAPTER III

NUMERICAL PROCEDURE

Two-dimensional, high-speed, turbulent flow simulations (with air as the fluid) are performed for a flow over a flat plate at two different free-stream Mach numbers (M_∞ = 2.25, 7.2). The simulations are performed using FLUENT, a commercial CFD software. The flow conditions and simulation setups used for these two Mach number cases are given below.

A $M_\infty = 2.25$

The free-stream conditions used for this case are obtained from the DNS study (Pirozzoli *et al.*, 2004). A free-stream temperature, T_∞, of 169.44 K and a free-stream unit Reynolds number, $Re_\infty/in.$, of $635,000/in.$ are used for this particular case. From the given free-stream conditions, the values of other flow variables at free-stream conditions are computed as follows:

$$U_\infty = M_\infty \sqrt{\gamma R T_\infty} \tag{3.1a}$$

$$\rho_\infty = \frac{Re_\infty/m\mu_\infty}{U_\infty} \tag{3.1b}$$

$$P_\infty = \rho_\infty R T_\infty \tag{3.1c}$$

where U_∞ is the velocity component along the plate, γ is the ratio of specific heats, ρ_∞ is the density, μ_∞ is the viscosity, P_∞ is the static pressure and R is the universal gas constant. To calculate μ_∞, the Sutherland's law (White, 2006) is used,

$$\mu_\infty = \mu_0 \left(\frac{T_\infty}{T_0}\right)^{3/2} \frac{T_0 + S}{T_\infty + S} \tag{3.2}$$

where $\mu_0 = 1.716 \times 10^{-5}$ kg/m-s, $T_0 = 273.11$ K and $S = 110.56$ K.

Figure 1 shows the two-dimensional computational domain used. In the DNS study (Pirozzoli *et al.*, 2004), a time-dependent, laminar compressible boundary layer similarity solution (White, 2006) is used as an inlet boundary condition. So for the present study, the region (Xa-Xb) is considered a laminar flow region. To induce laminar-to-turbulent transition like in the DNS study, a region of blowing and suction is introduced (region (Xb-Xc) in figure 1) wherein a time-dependent profile for normal velocity component is used. A relatively fine mesh is used in this region to capture the transition in the flow. Like in the DNS study, there are three subsequent zones namely, transition zone (Xc-Xd), turbulent zone (Xd-Xe) and the buffer zone (Xe-Xf). The zone (Xd-Xe) is where the turbulence develops and a relatively fine grid spacing is used to capture this development. Except for the blowing/suction region (Xb-Xc), adiabatic wall condition is used for all the other regions.

It should be noted that the above mentioned domain partitions hold for an unsteady simulation only. For a steady-state simulation, all the zones are turbulent zones and an adiabatic wall condition is used for all the zones.

The zone dimensions and grid spacings are shown in figure 1. In the y-direction, the first grid point is placed at a distance of 3.75×10^{-7} m, which corresponds to a y^+ of about 0.2. The dimensionless parameter y^+ is defined as $y^+ = \rho_w y u_\tau / \mu_w$, where ρ_w, μ_w are the density and viscosity of air at the wall and u_τ is the friction velocity.

The type of boundary conditions used for this flow simulation are summarized in Table 1.

For a 'Pressure inlet' boundary condition, the values of static pressure (P_∞),

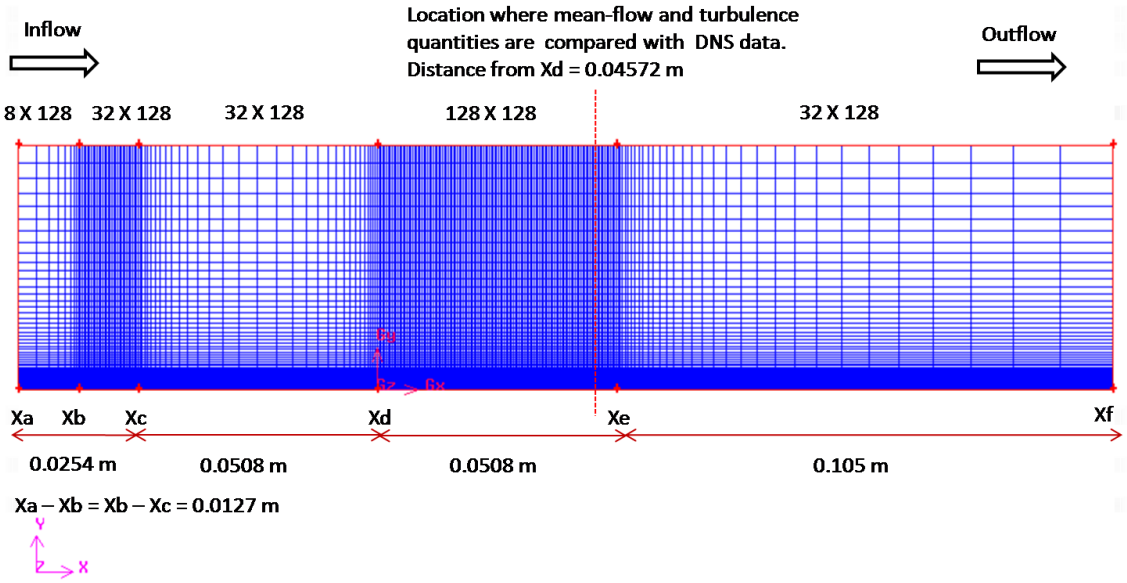

FIGURE 1. Computational domain, M_∞= 2.25 case

TABLE 1. Simulation Boundary Conditions, $M_\infty = 2.25$

Boundary	Condition
Inlet	Pressure inlet
Outlet	Pressure outlet
Top	Symmetry
Bottom	Adiabatic wall

total pressure and total temperature are specified using the following equations:

$$P_{total} = P_\infty \left(1 + \frac{\gamma - 1}{2} M_\infty^2\right)^{\frac{\gamma}{\gamma - 1}} \tag{3.3a}$$

$$T_{total} = T_\infty \left(1 + \frac{\gamma - 1}{2} M_\infty^2\right) \tag{3.3b}$$

In addition, an inlet turbulence condition has to be specified. For this study, turbulence intensity (defined as the ratio of the root-mean-square of the velocity fluctuation, u', to the free-stream velocity, U_∞) and turbulent viscosity ratio, μ_t/μ, are specified at the inlet. The values used for these quantities are 1 % and 0.1, repectively.

The 'Pressure outlet ' type of boundary condition in FLUENT requires the specification of backflow static pressure and backflow total temperature. For a supersonic flow, these quantitites at the outlet are typically computed by extraplolation. However, when the flow becomes locally subsonic, like in a boundary layer, the values input by the user are used for computations. The values of the backflow total temperature and backflow static pressure are the same as the values specified at the inlet (3.3a and 3.3b apply again).

The simulation settings are summarized below in Table 2 and the convergence criteria used for the simulations are summarized in Table 3.

For the grid adequacy study, two-dimensional steady-state turbulent flow simulations (using the SST turbulence model) on a two-inch flat plate are performed on three different grids using the flow and boundary conditions mentioned above. This study on a two-inch flat plate would yield a grid distribution that would be adequate for the turbulent zone (Xd-Xe) in figure 1. The grids are generated using GAMBIT, a commercial software. In each of these cases, the grid points in the flow direction are uniformly spaced and in the wall normal direction, the grid points are obtained by

TABLE 2. FLUENT Computational Settings

Settings	Choice
Fluid	Air
Simulation type	2d, steady
Solver	Density based
Formulation	Implicit
Molecular viscosity	Sutherland's law
Momentum	3^{rd} order MUSCL scheme
Turbulent kinetic energy	2^{nd} order upwind scheme
Turbulent dissipation rate	2^{nd} order upwind scheme

TABLE 3. Convergence Criteria

Variable	Residual
Mass	1e-06
x-velocity	1e-08
y-velocity	1e-08
Energy	1e-08
k	1e-08
ϵ or ω	1e-08

specifying the distance of the first grid point from the wall, y_w, and the total number of points. The three grids used are 64×64, 128×128 and 256×256. A 64×64 indicates that there are 64 cells in both streamwise and wall normal directions. The van Driest flat plate (White, 2006) theory is used to obtain a value of y_w that corresponds to a $y^+ \approx 1$. This value of y_w is used for the 64×64 grid.

Mean velocity ($u^+ = \widetilde{U}/u_\tau$, $\widetilde{U}$ is the Favre-averaged velocity), at a location 0.04572 m downstream of the inlet, is plotted (figure 2) for the three grids mentioned above. Except in the outer region of the boundary layer, the three grids yield identical results. To ensure sufficient points inside the boundary layer, a 128×128 grid is chosen for the turbulent zone (Xd-Xe) in figure 1.

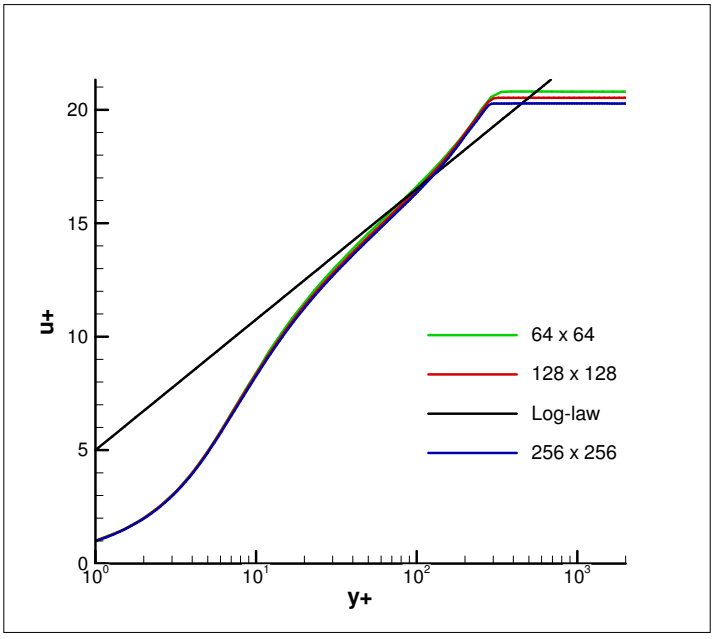

FIGURE 2. Grid adequacy study, M_∞= 2.25 case

B $M_\infty = 7.2$

The free-stream conditions used for this case are obtained from experimental data (Horstman & Owen, 1975). The free-stream conditions are: temperature $T_\infty = 59$ K, total temperature, T_{total}=667 K, wall temperature, $T_w = 310$ K, unit Reynolds number, $Re_\infty/cm = 1.09 \times 10^5$, static pressure, $P_\infty = 0.00673$ atm and total pressure, $P_{total} = 34$ atm.

The test model used in the experiment (Horstman & Owen, 1975) was a 10^o cone-ogive-cylinder, 330 cm long and 20.3 cm in diameter. The transition to turbulence was observed at around 80 cm downstream of inlet. Mean flow and turbulence quantities were measured at different stations (85 cm - 237 cm downstream of inlet) in the turbulent zone.

The two-dimensional computational domain used for a flow over a flat plate at $M_\infty = 7.2$ is shown below (figure 3). Unlike the $M_\infty = 2.25$ case, there is no partitioning of the domains into several zones with different grid spacings. The entire domain is considered a turbulent zone. In the flow direction, there are 257 grid points with the first grid point placed at a distance of 10^{-3} m from the inlet. There are 129 grid points in the wall-normal direction with the first grid point placed at a distance, y_w of 10^{-6} m from the bottom surface. The mean flow and turbulence quantities obtained from this study is compared with the experimental data at $x = 2.37m$.

The type of boundary conditions used for this flow simulation are summarized in Table 4. The various flow variables to be specified for the 'Pressure inlet' and 'Pressure outlet' type boundary conditions are described in the previous section, and the values of these variable are stated above. Similar to the $M_\infty = 2.25$ case, a turbulence intensity of 1 % and a turbulent viscosity ratio of 0.1 are specified at the inlet.

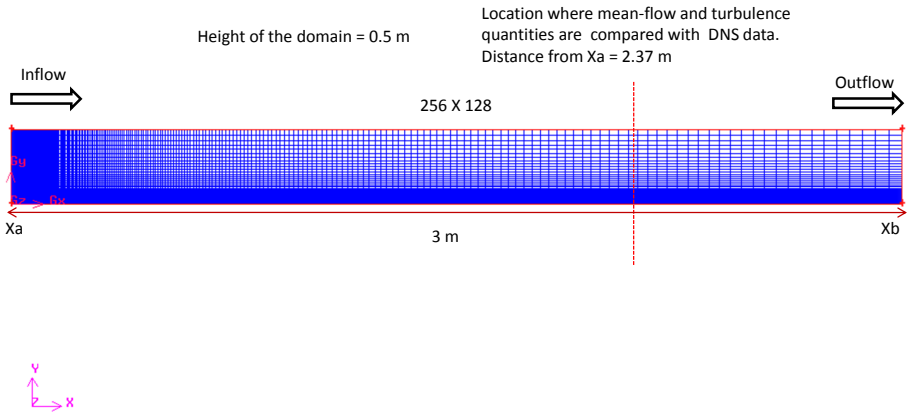

FIGURE 3. Computational domain, M_∞= 7.2 case

TABLE 4. Simulation Boundary Conditions, $M_\infty = 7.2$

Boundary	Condition
Inlet	Pressure inlet
Outlet	Pressure outlet
Top	Symmetry
Bottom	Constant temperature wall

The simulation settings are summarized in Table 2 and the convergence criteria used for the simulations are summarized in Table 3.

For the computational domain shown in figure 3, a grid adequacy study is performed. Three grids, 256×64 grid with $y_w = 10^{-6}$ m, 256×128 with $y_w = 10^{-6}$ m, and 256×128 with $y_w = 5 \times 10^{-7}$ m, are used for this study. A 256×64 indicates that there are 256 cells in the flow direction and 64 cells in the wall-normal direction. For each of these grids the distance of the first grid point from the inlet in the flow direction is 10^{-3} m. The mean velocity, after using the van Driest transformation (White, 2006), is plotted against y^+ at $x = 2.37$ m (figure 4). Like in the Mach 2.25 case, to ensure sufficient points inside the boundary layer, a 256×128 grid with y_w 10^{-6} m is chosen for subsequent flow computations.

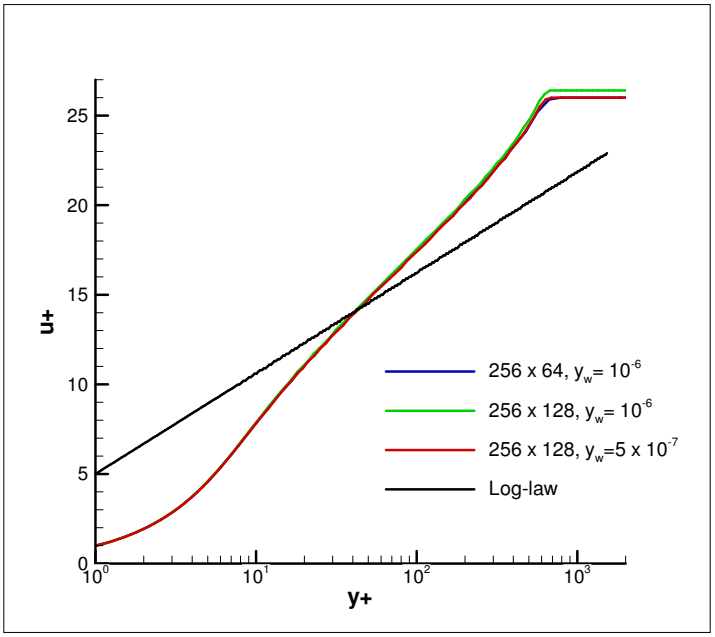

FIGURE 4. Grid adequacy study, M_∞= 7.2 case

CHAPTER IV

RESULTS

As mentioned in Chapter II, four studies are performed to address the objectives of this research:

1. Performance of the standard $k-\epsilon$ and $k-\omega$ turbulence models.
2. The effect of turbulent transport coefficients ($\sigma_k, \sigma_\epsilon, \sigma, \sigma^*$) and the Boussinesq closure coefficient (C_μ) on boundary layer prediction.
3. Performance of the new model with realizability-based correction to the Boussinesq coefficient and corresponding modifications to transport coefficients.
4. The role of turbulent Prandtl number in temperature and density predictions.

A Study 1: Performance of the standard $k-\epsilon$ and $k-\omega$ turbulence models

The performance of two popular two-equation models namely, standard $k-\epsilon$ and $k-\omega$ models, in predicting a supersonic boundary layer is studied. Two-dimensional steady-state simulations using these turbulence models are performed for a flow over a flat plate at M_∞= 2.25. The computational domain used for this Mach number is described in Chapter III. The results from these simulations are compared with DNS data (Pirozzoli *et al.*, 2004) at the location shown in figure 1 (reference location) and the performance is evaluated.

The mean velocity obtained from standard $k-\epsilon$ model and $k-\omega$ model computations are plotted at the reference location in figure 5. Here, u^+ corresponds to the ratio of van Driest transformed (White, 2006) mean velocity to friction velocity, u_τ, and $y^+ = \rho_w y u_\tau/\mu_w$, where ρ_w, μ_w are the density and viscosity of air at wall

conditions.

The $k-\omega$ model performance is much better compared to the standard $k-\epsilon$ model in the log-layer region of a compressible flow boundary layer. The standard $k-\epsilon$ model overpredicts the value of friction velocity, u_τ, which results in a smaller value of the slope in the log-layer region and an increase in the boundary layer thickness. Except for y^+ values between 10 and 100, the $k-\omega$ model result agrees well with the DNS data.

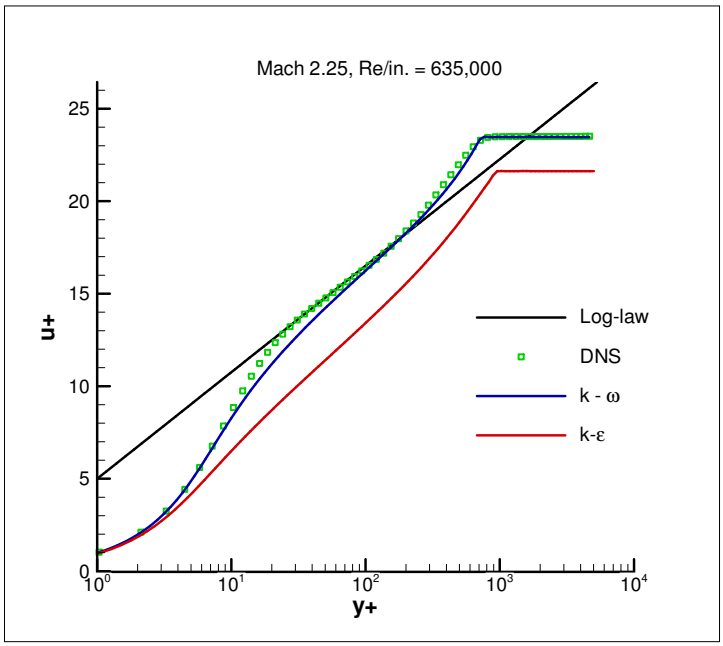

FIGURE 5. Performance of $k-\epsilon$ and $k-\omega$ models: u^+ vs. y^+, $M_\infty = 2.25$

Figure 6 shows the variation of turbulent kinetic energy at the reference location for the two models simulated. Both the standard $k-\epsilon$ and $k-\omega$ models overpredict the value of k. However, the performance of $k-\omega$ model is better compared to the $k-\epsilon$ model, especially in the near-wall region of the boundary layer. The $k-\omega$ model also performs better in predicting the turbulent viscosity, μ_t, values in the outer region of the boundary layer (figure 7).

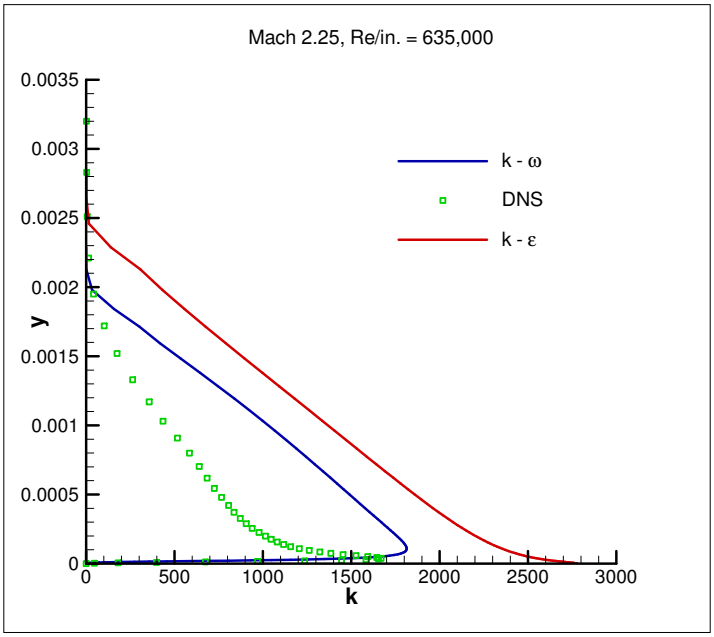

FIGURE 6. Performance of $k-\epsilon$ and $k-\omega$ models: k vs. y, $M_\infty = 2.25$

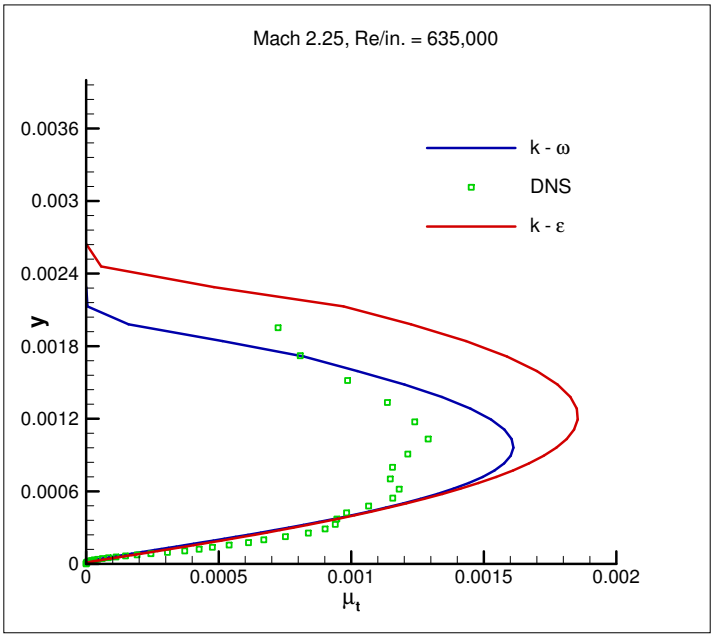

FIGURE 7. Performance of $k-\epsilon$ and $k-\omega$ models: μ_t vs. y, $M_\infty = 2.25$

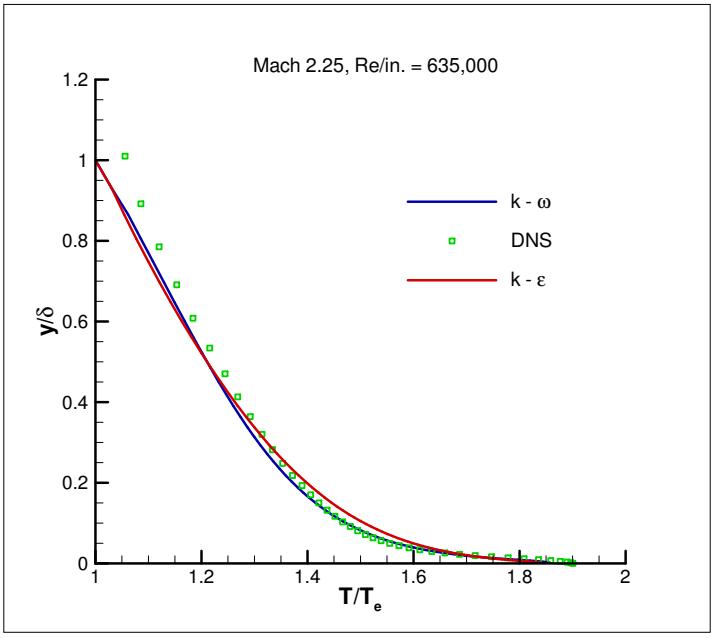

FIGURE 8. Performance of $k-\epsilon$ and $k-\omega$ models: T/T_e vs. y/δ, $M_\infty = 2.25$

Plots of T/T_e and ρ/ρ_e against y/δ are shown in figures 8 and 9, respectively. Here, T_e represents the value of temperature at the edge of the boundary layer and δ is the boundary layer thickness. The temperature and density predictions of the $k-\omega$ and the standard $k-\epsilon$ models are almost identical in the outer region of the boundary layer. However, the near-wall performance of the $k-\omega$ model is better compared to that of the standard $k-\epsilon$ model.

It is clear from this study that the $k-\omega$ model performs consistently better than the $k-\epsilon$ model in predicting the boundary layer for Mach 2.25 case. Hence, for the subsequent studies the $k-\omega$ model is used as the reference model.

In order to study the Reynolds number effect on $k-\omega$ model flow predictions, mean velocity is plotted at the outlet of the computational domain (figure 1). Figure 10 shows that the log-layer mean velocity prediction improves with an increase in the

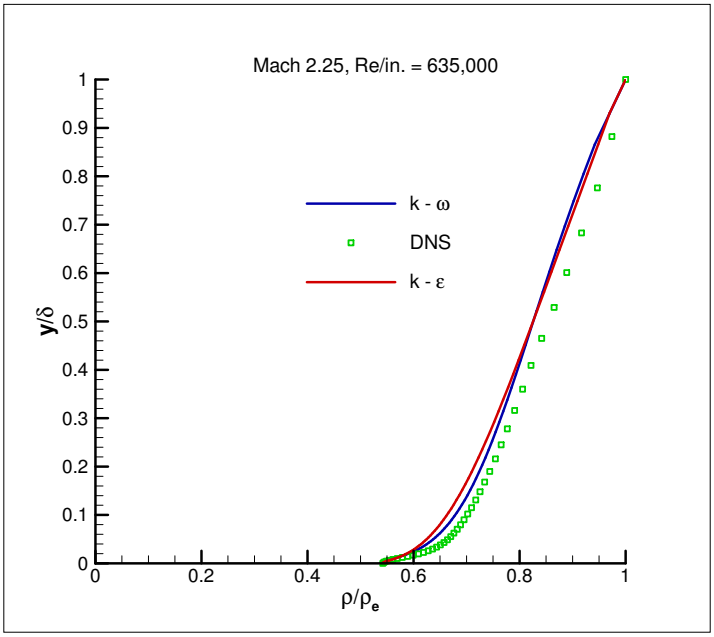

FIGURE 9. Performance of $k-\epsilon$ and $k-\omega$ models: ρ/ρ_e vs. y/δ, $M_\infty = 2.25$

Reynolds number value. The other flow quantities are not shown here due to the unavailability of DNS (Pirozzoli *et al.*, 2004) data at the outlet. However, investigations in this research show that an improvement in the mean velocity prediction at a particular location improves the mean temperature prediction as well. Hence, with an increase in the Reynolds number, an improved mean temperature prediction is expected.

From this point forward, for the Mach 2.25 case, the focus is on the reference location for the other studies.

B Study 2: The effect of turbulent transport coefficients $(\sigma_k, \sigma_\epsilon, \sigma, \sigma^*)$ and the Boussinesq closure coefficient (C_μ) on boundary layer prediction

Case1: Effect of change in C_μ value

The default value of C_μ for $k-\epsilon$ model (or β^* for $k-\omega$ model) is 0.09. To analyze

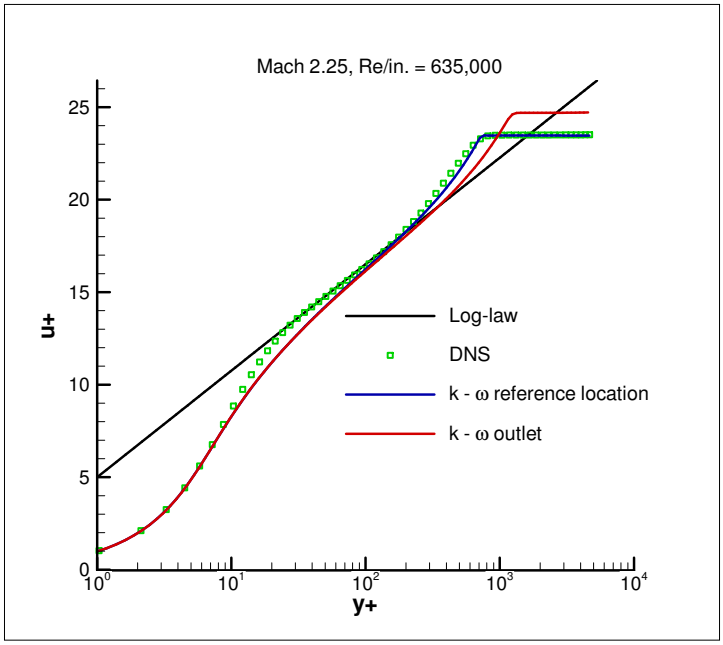

FIGURE 10. Reynolds number effect on $k-\omega$ model mean velocity prediction, $M_\infty = 2.25$

the effect of C_μ on the boundary layer, a flow simulation (at $M_\infty = 2.25$ and boundary conditions described in Chapter III) using the $k-\omega$ model with $\beta^* = 0.05$ is performed.

Figure 11 shows a plot of u^+ against y^+ at the reference location for β^*=0.05 and 0.09. Clearly, β^* controls the slope in the log-layer region of the boundary layer. A decrease in the value of β^* increases the value of friction velocity u_τ which results in a decrease in the slope in the log-layer region. A increased value of u_τ also increases the boundary layer thickness.

The effect of changing β^* is not restricted to velocity in the boundary layer. Figures 12, 13 show plots of k versus y and μ_t versus y at the reference location, respectively. In the log-layer region, $k \approx u_\tau^2/\sqrt{\beta^*}$ (Wilcox, 1994). So a decrease in the value of β^* and a consequent increase in the value of u_τ causes an increase in the

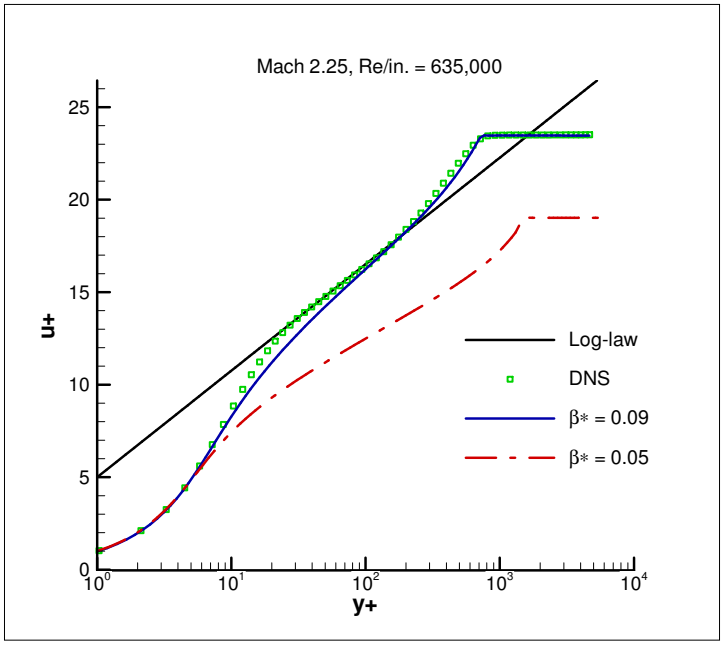

FIGURE 11. Effect of Boussinesq coefficient: u^+ vs. y^+, $M_\infty = 2.25$

values of k and μ_t ($\mu_t \propto k^2$).

Case2: Effect of transport coefficients: σ_ω (or $1/\sigma$) and σ_k (or $1/\sigma^*$)

The value of C_μ or β^* is reduced to accommodate the realizability requirement. If β^* is changed in isolation, κ may decrease (2.52b) leading to a decreased slope (11) which indicates higher k (12) and μ_t (13) in the log-layer. For a decrease in β^*, there has to be an increase in the value of σ_ω for (2.52b) to be true. The value of σ_ω obtained from (2.52b) is used in this study. The modification of the other transport coefficient, σ_k, is dictated by a different requirement. Investigations from this study show that σ_k controls the boundary layer thickness, δ. In order to obtain reasonable δ, σ_k is varied such that

$$\left(\frac{\sigma_\omega}{\sigma_k}\right)_{C_\mu=0.09} = \left(\frac{\sigma_\omega}{\sigma_k}\right)_{C_\mu variable} \tag{4.1}$$

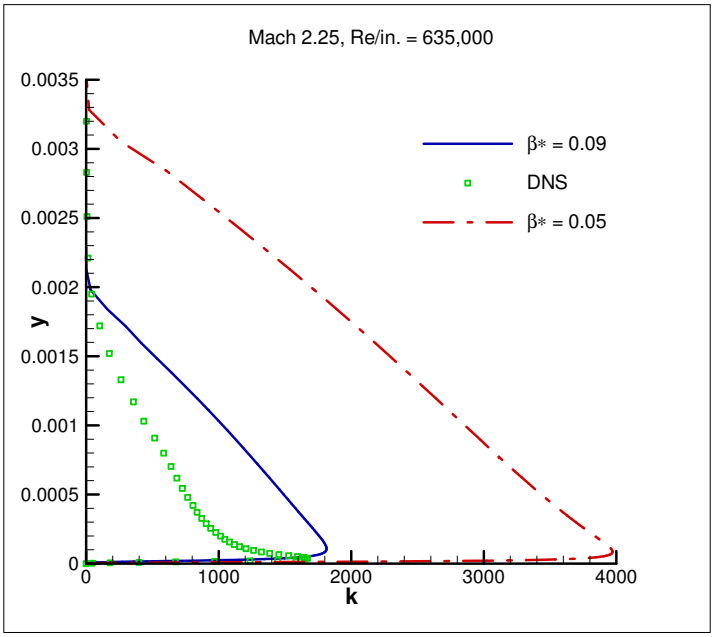

FIGURE 12. Effect of Boussinesq coefficient: k vs. y, $M_\infty = 2.25$

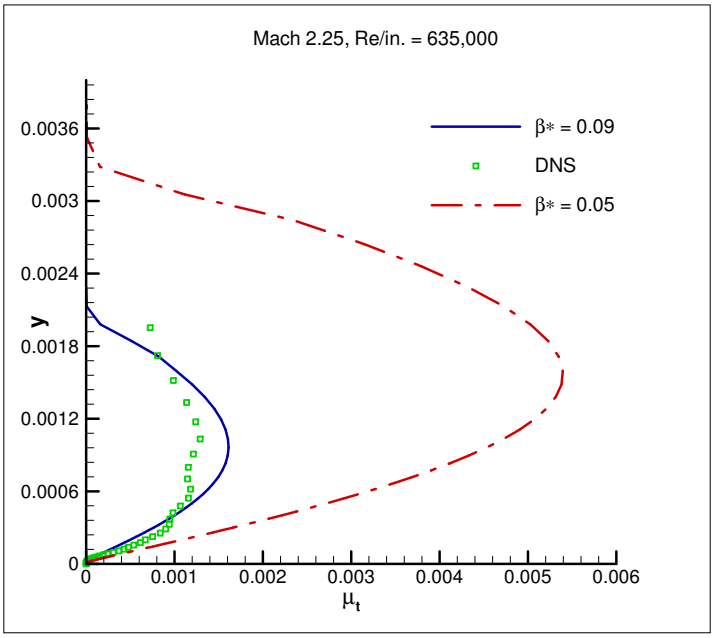

FIGURE 13. Effect of Boussinesq coefficient: μ_t vs. y, $M_\infty = 2.25$

Figures 14, 15 and 16 show the velocity, turbulent kinetic energy and turbulent viscosity profiles (at a location shown in figure 1). The variation in σ_ω results in a decrease in the value of u_τ and hence there is an increase in the slope in the log-layer region and a decrease in the boundary layer thickness. Also, a reduced u_τ, results in a lower k and μ_t.

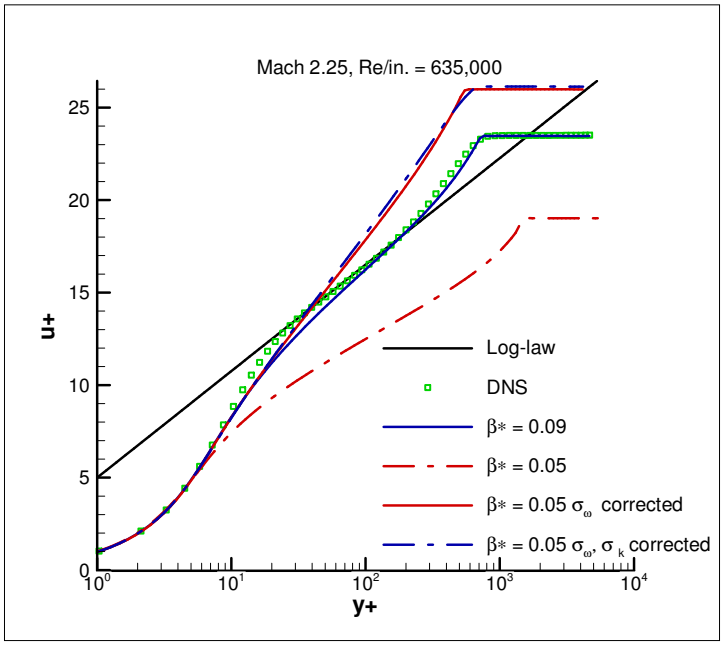

FIGURE 14. Effect of transport coefficients: u^+ vs. y^+, $M_\infty = 2.25$

The effect of variation of σ_k is subtle and is restricted to the outer region of the boundary layer. A slightly improved prediction in k and μ_t is observed towards the edge of the boundary layer.

It can thus be concluded that changing σ_k and σ_ω along the lines of (2.52b) as we change C_μ is crucial for capturing the correct boundary layer behavior.

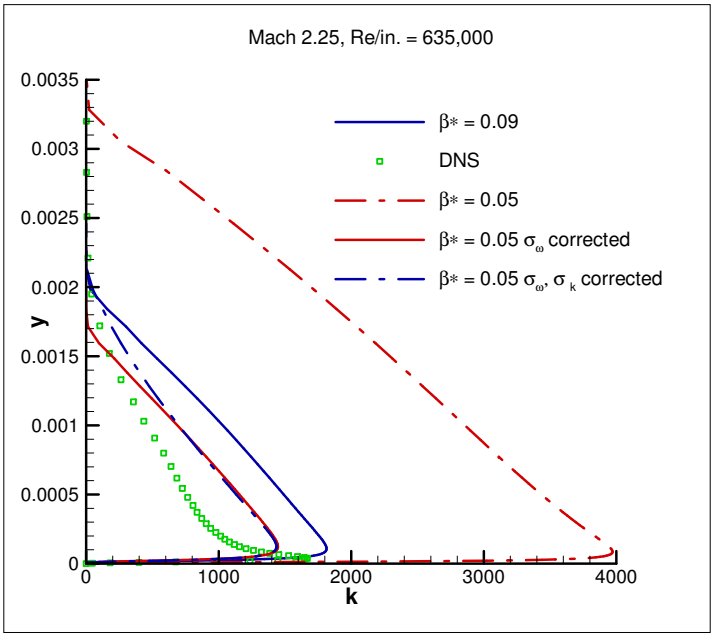

FIGURE 15. Effect of transport coefficients: k vs. y, $M_\infty = 2.25$

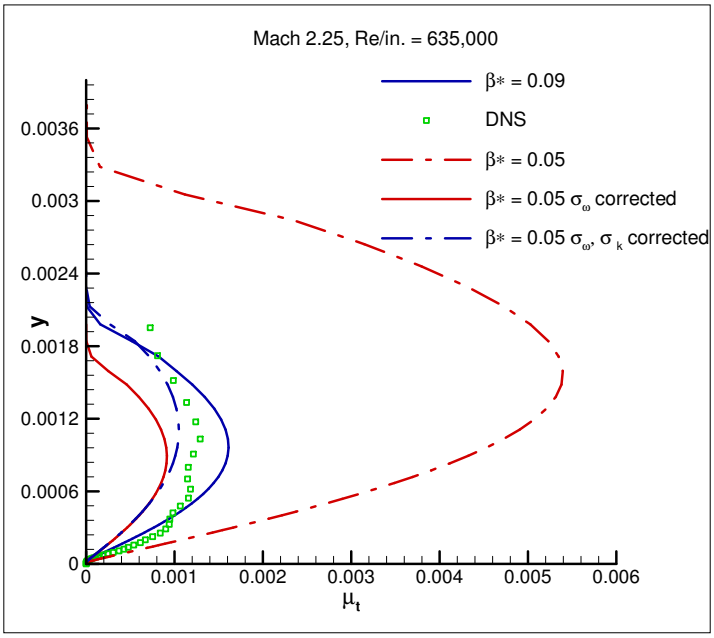

FIGURE 16. Effect of transport coefficients: μ_t vs. y, $M_\infty = 2.25$

C Study 3: Performance of the new model with realizability-based correction to the Boussinesq coefficient and corresponding modifications to transport coefficients

The variations in Boussinesq closure coefficient C_μ (or β^*) and transport coefficients σ_k, σ_ω are described in Chapter II. The performance of the $k-\omega$ model with variable closure and transport coefficients is evaluated for two-dimensional compressible turbulent boundary layer flows at M_∞= 2.25, 7.2. The computational setups used for these two Mach number cases are described in Chapter III.

1 M_∞=2.25

Table 5 shows the various cases considered in this study. The results from these cases are compared with the results obtained from the standard $k-\omega$ model and DNS (Pirozzoli *et al.*, 2004) data at the reference location.

TABLE 5. C_μ Variation Study, $M_\infty = 2.25$

Case 1	Variable β^* σ_ω, σ_k variable
Case 2	Variable β^*, σ_ω= 2, $\sigma_k = 2$
Case 3	Variable β^*, σ_ω variable, $\sigma_k = 2$
Case 4	Variable β^*, σ_ω variable, $\sigma_k = 2 \times \sigma_\omega$

Figure 17 shows a plot of u^+ versus y^+ data for DNS (Pirozzoli *et al.*, 2004), $k-\omega$ model and the cases mentioned in Table 5. It can be seen that the performance of the $k-\omega$ model and variable β^* model (case 1) are identical. The variable β^* model predicts the boundary layer thickness correctly while the other variational models (case 2-case 4) predict a slightly lower boundary layer thickness. It can thus be concluded that, for mean velocity, the effect of variations in transport coefficients,

σ_ω, σ_k, is restricted to the outer region of the boundary layer.

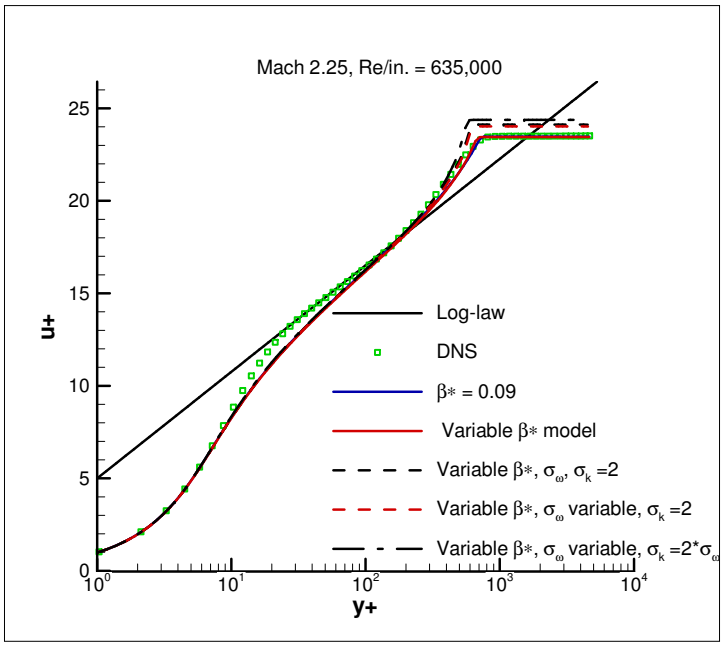

FIGURE 17. Variable β^* model evaluation: u^+ vs. y^+, $M_\infty = 2.25$

A plot of k versus y for the various cases considered is shown in figure 18. It can be seen that the performance of the variable β^* model is as good as that of the $k-\omega$ model. In fact, the performance is slightly better in the outer region of the boundary layer. The variations in transport coefficients: case 2-case 4, result in slightly lower peak values of k close to the wall and reduced values of k in the outer region of the boundary layer.

A similar performance is seen in the prediction of μ_t (figure 19). The variations in transport coefficients (case 2-case 4), σ_ω, σ_k clearly result in lower values of μ_t in the outer region of the boundary layer and also lower peak values. It appears, that an increase in the value of σ_k results in a decrease in the value of μ_t in the outer region of the boundary layer.

The temperature and density profiles versus y are shown in figures 20 and 21.

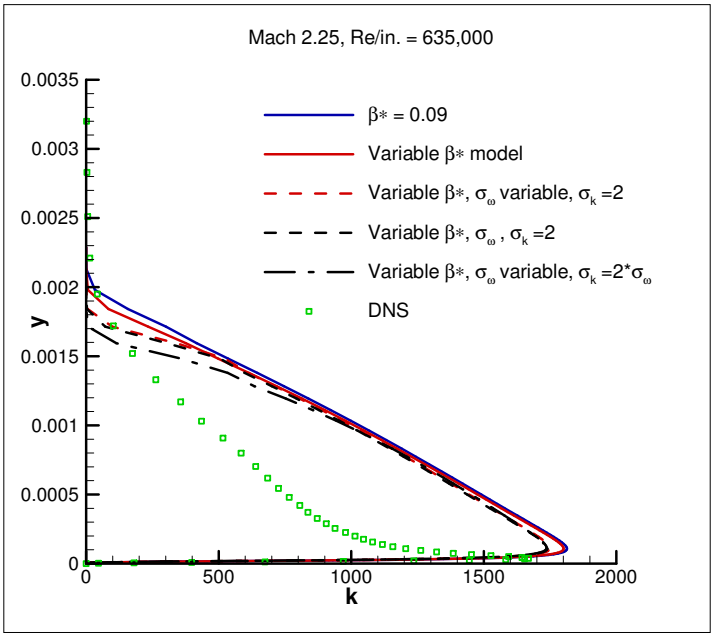

FIGURE 18. Variable β^* model evaluation: k vs. y, $M_\infty = 2.25$

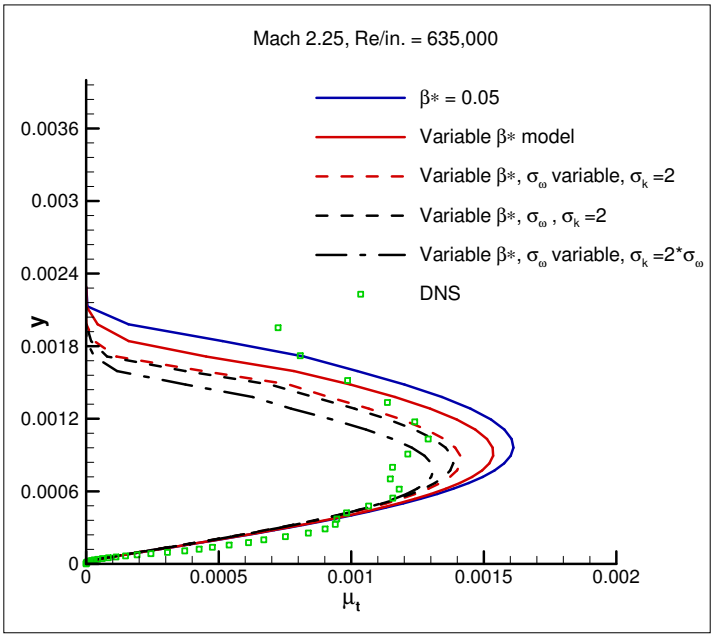

FIGURE 19. Variable β^* model evaluation: μ_t vs. y, $M_\infty = 2.25$

The variable β^* model results in a slightly improved temperature prediction in the outer region of the boundary layer. The variable β^* model's density prediction is almost identical to that of the $k-\omega$ model.

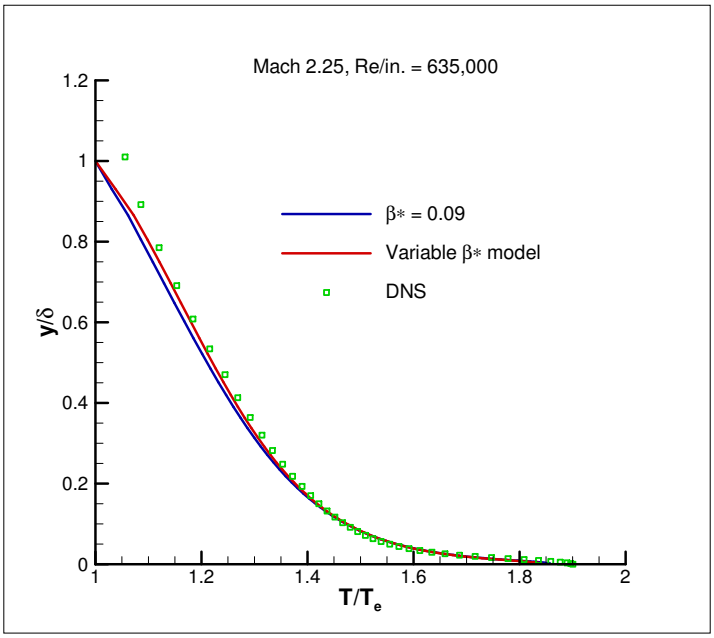

FIGURE 20. Variable β^* model evaluation: T/T_e vs. y/δ, $M_\infty = 2.25$

2 M_∞=7.2

The performances of the $k-\omega$ model and the variable β^* model (case 1 in Table 5) are compared with the available experimental data (Horstman & Owen, 1975). A plot of u^+ versus y^+ is shown in figure 22. Clearly, the performances of the $k-\omega$ model and the variable β^* model are identical. Except for y^+ values between 10 and 100, the results from the $k-\omega$ model and the variable β^* model are in reasonable agreement with the experimental data.

Figures 23 and 24 show plots of temperature and density variations with y. Similar performances are observed for the $k-\omega$ and the variable β^* model.

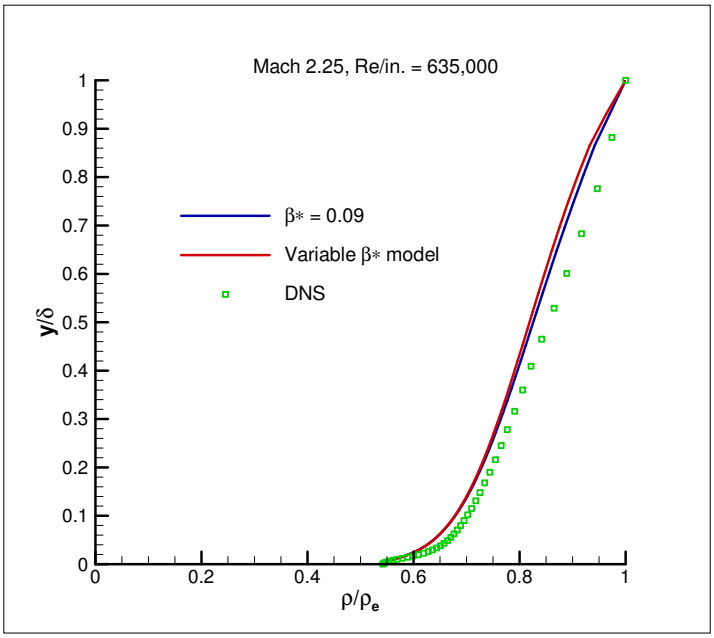

FIGURE 21. Variable β^* model evaluation: ρ/ρ_e vs. y/δ, $M_\infty = 2.25$

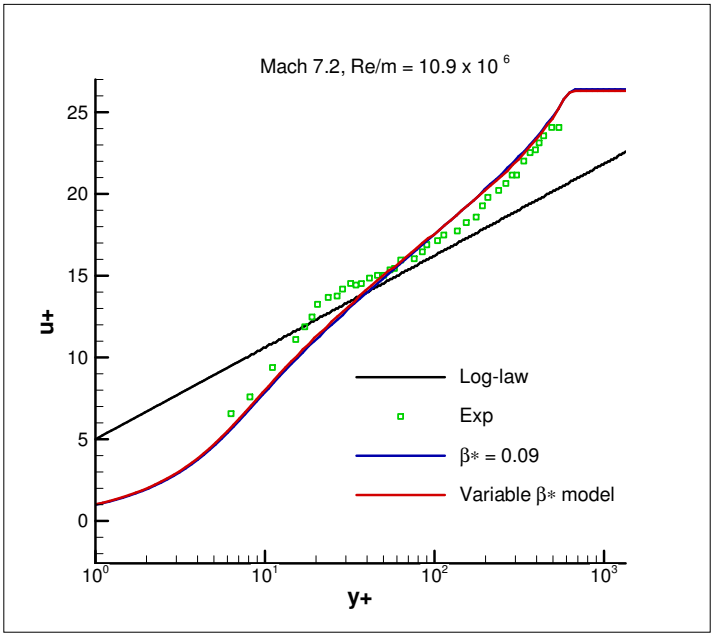

FIGURE 22. Variable β^* model evaluation: u^+ vs. y^+, $M_\infty = 7.2$

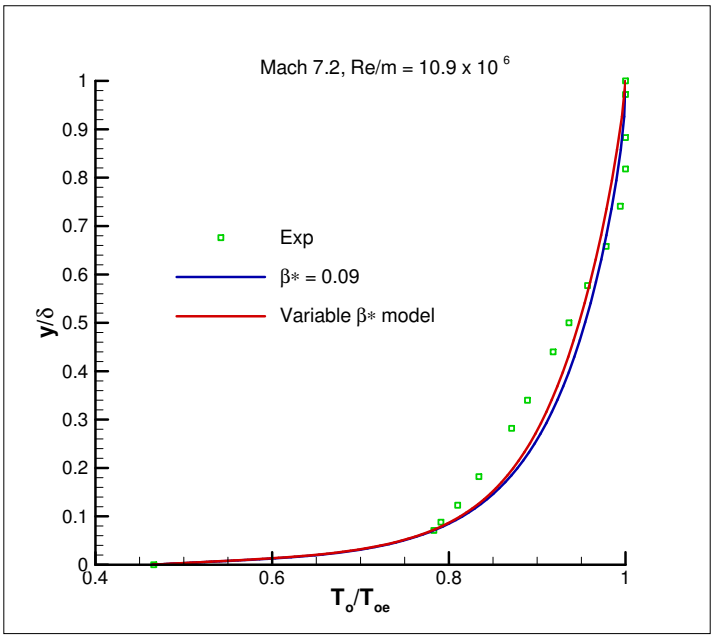

FIGURE 23. Variable β^* model evaluation: T/T_e vs. y/δ, $M_\infty = 7.2$

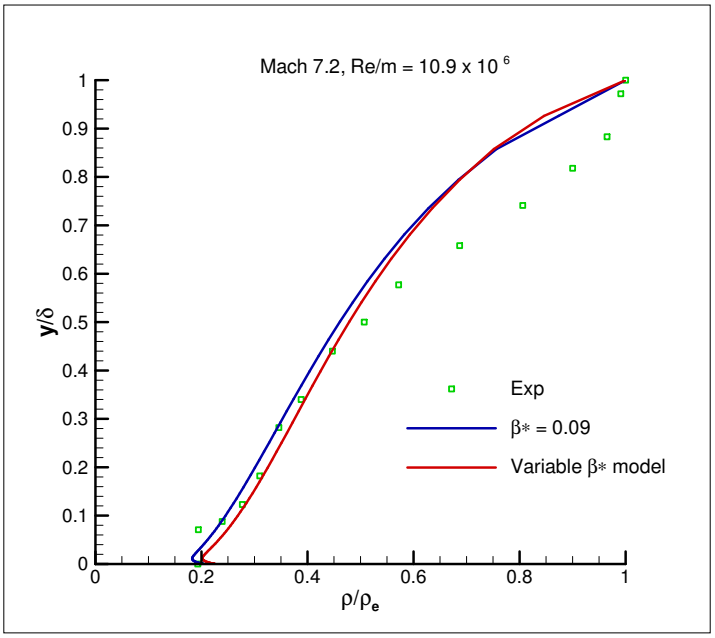

FIGURE 24. Variable β^* model evaluation: ρ/ρ_e vs. y/δ, $M_\infty = 7.2$

The performance of another variable β^* model, based on production to dissipation of kinetic energy ratio of 1.6, is tested for both Mach 2.25 and Mach 7.2 cases. The results are identical to that shown above.

Thus, the variable β^* model, which produced significant improvements for bluff body flows (Lakshmipathy, 2008), shows minor improvements for the flat plate simulations. The model performs as good as the standard $k-\omega$ model and in some cases better than the standard $k-\omega$ model. Also, there is no significant change in the boundary layer behavior at higher Mach numbers.

D Study 4: The role of turbulent Prandtl number in temperature and density predictions

In high-speed turbulent boundary layers, due to the interaction between flow and thermodynamic variables, temperature and density statistics must also be accurately predicted. In this study, the effect of turbulent Prandtl number, Pr_t, on mean temperature and density predictions is examined. First, a range of Pr_t values (0.7-1.15) are considered and then the effect of Pr_t variation across the boundary layer is studied.

Two-dimensional, steady-state, compressible flow simulations using the $k-\omega$ model are performed for a flow over at flat plate at $M_\infty = 2.25, 7.2$. The flow conditions and computational setups are described in Chapter III.

The temperature predictions for various Pr_t values is shown in figure 25. The near-wall prediction is shown in figure 26. It appears that for a Pr_t value less than the default value of 0.85, the near-wall temperature is underpredicted and for Pr_t greater than 0.85, the temperature is overpredicted. Towards, the edge of the boundary layer, temperature prediction with Pr_t of 0.7 is slightly better compared to that

of the standard $k-\omega$ model.

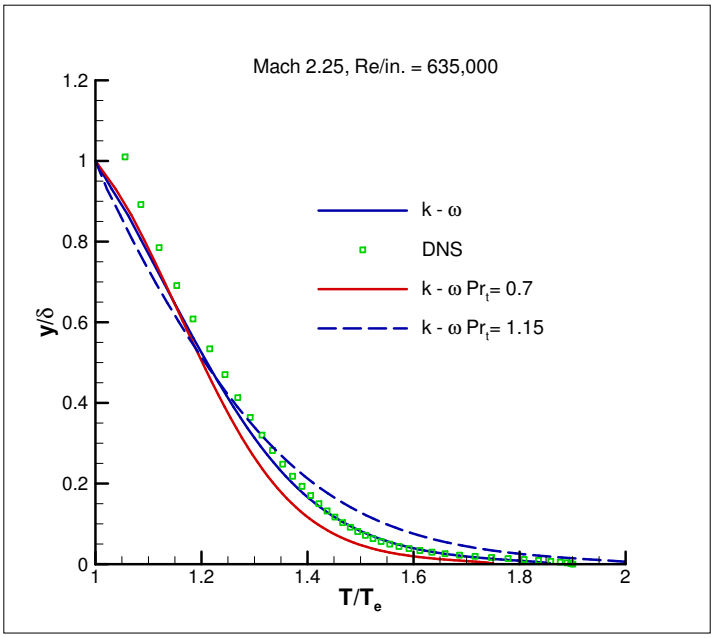

FIGURE 25. Effect of Pr_t: T/T_e vs. y/δ, $M_\infty = 2.25$

Figure 27 shows the variation of density across the boundary layer for various Pr_t values. Unlike the temperature predictions, the density is underpredicted for higher Pr_t value close to the wall and close to the free-stream, the density prediction improves at higher Pr_t. This is consistent with the fact that temperature and density are inversely related for a constant pressure flow (2.4).

These observations indicate that a fixed value of Pr_t across the boundary layer is not enough to obtain accurate temperature and density predictions simultaneously. A variation in Pr_t value across the boundary layer is required to obtain reasonably accurate temperature and density predictions.

The turbulent Prandtl number variation is achieved by using the Rotta's model (2.54). For the Mach 2.25 case, this variation is used only in the turbulent zone

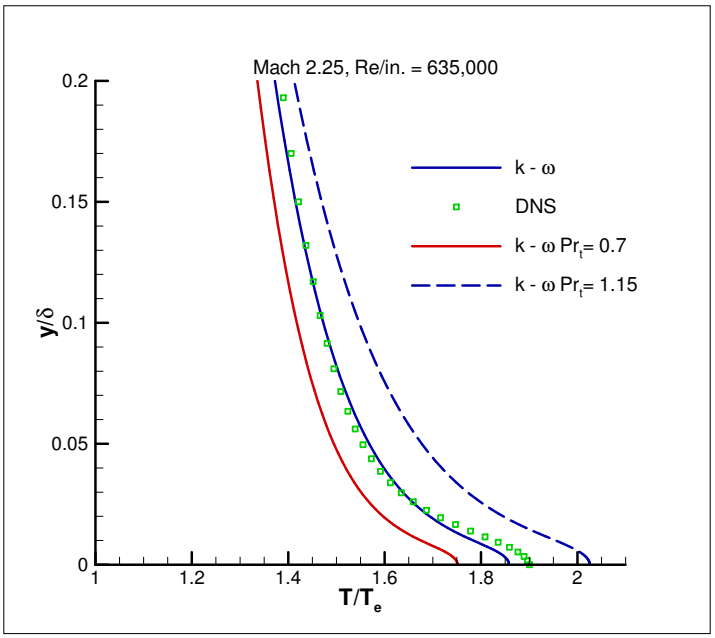

FIGURE 26. Effect of Pr_t: near-wall T/T_e vs. y/δ, $M_\infty = 2.25$

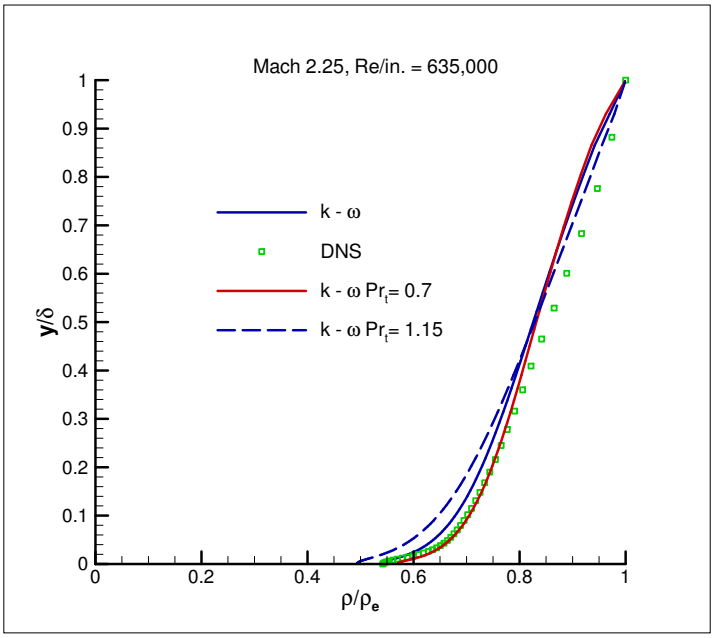

FIGURE 27. Effect of Pr_t: ρ/ρ_e vs. y/δ, $M_\infty = 2.25$

(Xd-Xe) in figure 1. The value of δ is obtained from a steady-state simulation using the $k-\omega$ model (without variation in Pr_t) at the location shown in figure 1.

Plots of T/T_e and ρ/ρ_e against y/δ are shown in figures 28, 29 and 30, respectively. It appears that the temperature and density predictions with and without Pr_t variation are almost identical. A closer look (figure 29) indicates that the temperature prediction at the wall improves when the Pr_t variation is used.

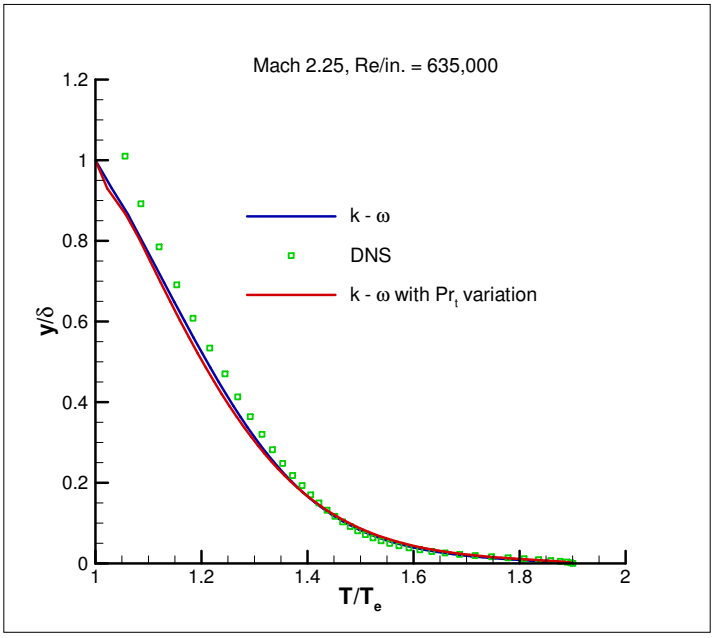

FIGURE 28. Variable Pr_t: T/T_e vs. y/δ, $M_\infty = 2.25$

Unlike the Mach 2.25 case, the Pr_t variation is used in the entire domain (figure 3) for the Mach 7.2 case. The value of δ is obtained from a steady-state simulation using the $k-\omega$ model at $x = 2.37$ m.

Figure 31 shows a plot of non-dimensional total temperature (T_o/T_{oe}) versus y/δ. The total temperature values are closer to the experimental data (Horstman & Owen, 1975) in the range $y/\delta = 0.1 - 0.2$ when Pr_t variation is used. Otherwise, the performance of the $k-\omega$ model with and without the Pr_t variation appear to

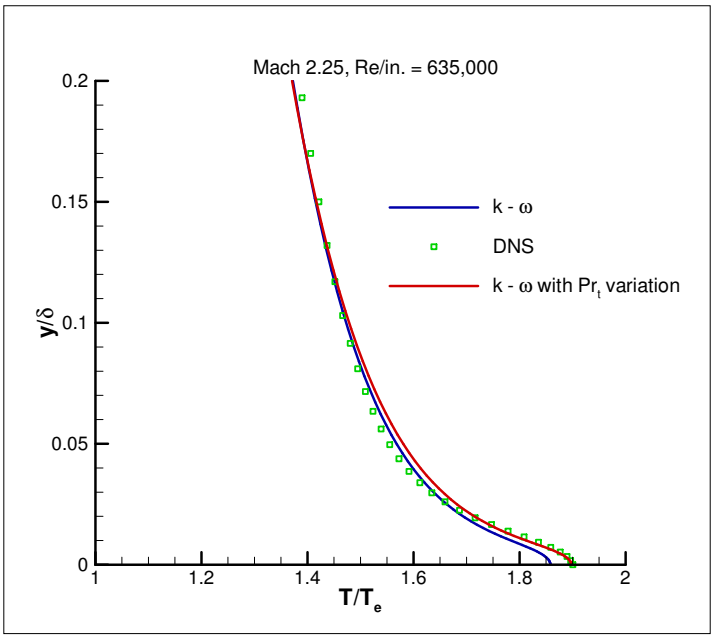

FIGURE 29. Variable Pr_t wall prediction: T/T_e vs. y/δ, $M_\infty = 2.25$

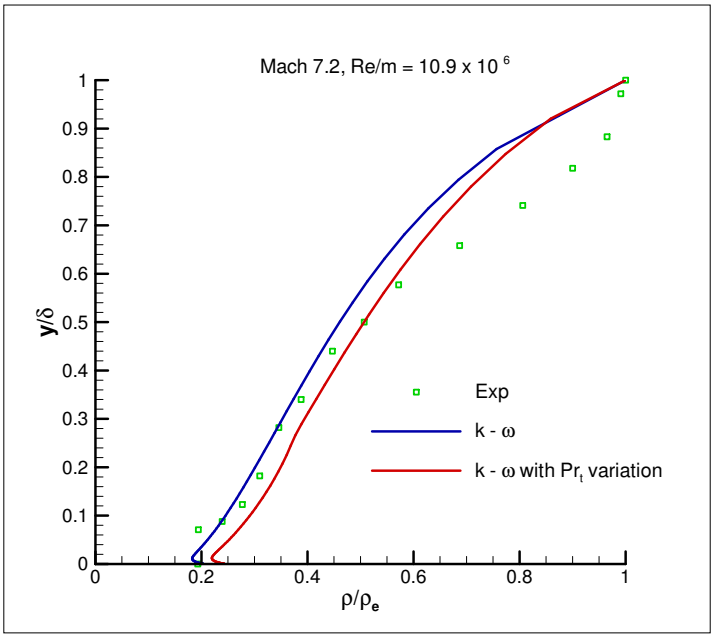

FIGURE 30. Variable Pr_t: ρ/ρ_e vs. y/δ, $M_\infty = 2.25$

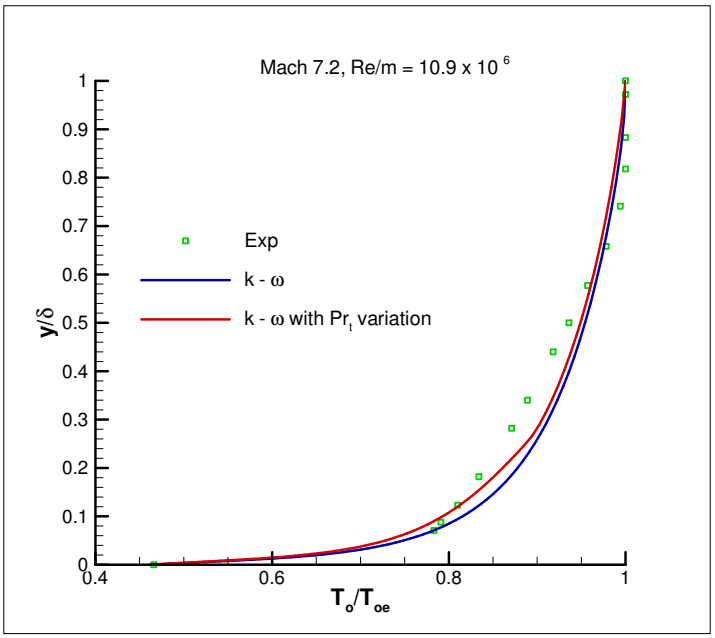

FIGURE 31. Variable Pr_t: T/T_e vs. y/δ, $M_\infty = 7.2$

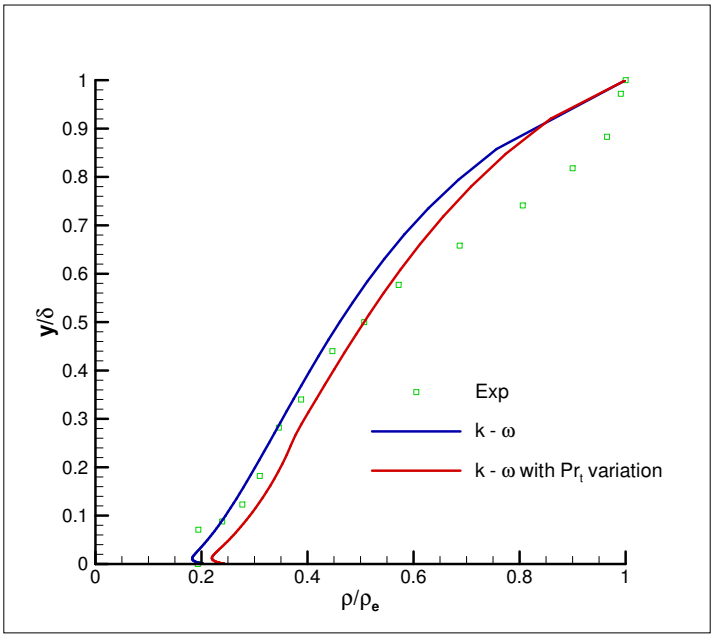

FIGURE 32. Variable Pr_t: ρ/ρ_e vs. y/δ, $M_\infty = 7.2$

be identical. The use of Pr_t variation results in a slightly increased values of density across the boundary layer (figure 32).

CHAPTER V

CONCLUSIONS

In the previous chapter, the performance of standard $k-\epsilon$ and $k-\omega$ models was tested in a Mach 2.25 boundary layer. Also, the effect of various transport coefficients ($\sigma_k, \sigma_\epsilon, \sigma, \sigma^*$) and Boussinesq coefficient (C_μ) on boundary layer prediction was studied. Further, the performance of the new realizability-based model was examined in Mach 2.25 and 7.2 boundary layers. Finally, the role of turbulent Prandtl number (Pr_t) in temperature and density predictions was studied. The conclusions from these studies are presented in this chapter.

A Performance of the standard $k-\epsilon$ and $k-\omega$ turbulence models

From the u^+ versus y^+ plot, it can be inferred that the standard $k-\epsilon$ model overpredicts the value of u_τ. This leads to a reduced slope in the log-layer region and an increase in the boundary layer thickness. Both the standard $k-\epsilon$ and $k-\omega$ models overpredict the value of k (and hence the value of μ_t) in the boundary layer. However, the $k-\omega$ model performance is better very close to the wall. The mean temperature and mean density plots also show that the $k-\omega$ model's near-wall performance is better compared to that of the $k-\epsilon$ model. Overall, the results from this study show that $k-\omega$ model performs better in a Mach 2.25 boundary layer.

For the $k-\omega$ model, an increase in the Reynolds number value leads to an improved prediction of mean velocity and temperature for a Mach 2.25 boundary layer. This indicates that the $k-\omega$ model is better suited for high-speed boundary layer flows.

B The effect of turbulent transport coefficients ($\sigma_k, \sigma_\epsilon, \sigma, \sigma^*$) and the Boussinesq closure coefficient (C_μ) on boundary layer prediction

It appears that a decrease in the value of C_μ results in an overprediction of u_τ. The value of k is approximately $u_\tau^2/\sqrt{C_\mu}$ in the log-layer region of a boundary layer. So a decrease in the value of C_μ and a consequent increase in the value of u_τ results in a significant overproduction of k in the boundary layer. A decrease in C_μ value and a corresponding change in the transport coefficient σ_ω improves the boundary layer performance. However, the value of u_τ and hence the values of k and μ_t are underpredicted. The effect of variation in σ_k is subtle and restricted to the outer region of the boundary layer. From this study, it can be concluded that a C_μ reduction must always be accompanied by corresponding changes in transport coefficients.

C Performance of the new model with realizability-based correction to the Boussinesq coefficient and corresponding modifications to transport coefficients

A plot of u^+ versus y^+ for Mach 2.25 case shows that the performances of the new realizability based model and the $k-\omega$ are identical. The new model shows slightly improved mean temperature prediction and the density prediction is the same as that of the $k-\omega$ model. The realizability based corrections come into play in regions with high strain rates. For a simple flow over a flat plate, however, C_μ assumes its constant value of 0.09 through most part of the boundary layer. A slightly reduced value of C_μ is seen close to the edge of boundary layer. This results in a slightly improved predictions of k and μ_t in the outer region of the boundary layer.

The plots of k versus y and μ_t versus y show that a realizability based correction to C_μ alone will not suffice. The modifications to transport coefficients (in addition to C_μ modification) improves the prediction of k and μ_t in the outer region of the

boundary layer.

For Mach 7.2 case, a similar behavior is observed. The plots of $\widetilde{U}$, ρ and $\widetilde{T}$ show that the performances of the new model and the $k-\omega$ model are similar.

Thus, the new model, which showed improved predictions for flow around bluff bodies (Lakshmipathy, 2008), performs as good as the standard $k-\omega$ model for Mach 2.25, 7.2 boundary layers.

D The role of turbulent Prandtl number in temperature and density predictions

For the Mach 2.25 case, temperature is underpredicted close to the wall and overpredicted close to the free-stream for Pr_t values lower than 0.85 and vice-versa for Pr_t values greater than 0.85. The density predictions are inversely related to the temperature predictions due to the absence of pressure gradient along the flow direction.

The use of Pr_t variation improves the temperature prediction at the wall for Mach 2.25 case. Otherwise, the temperature and density predictions appear to be identical with and without Pr_t variation.

For Mach 7.2 case, the total temperature prediction improves in the range $y/\delta = 0.1-0.2$ and the prediction is the same as the $k-\omega$ model elsewhere. The use of Pr_t variation results in a slightly increased values of density across the boundary layer.

Thus, the results indicate that Pr_t variation is required to achieve reasonably accurate temperature and density predictions close to the wall. The Pr_t variation has no significant effect on outer region predictions. Also, improved modeling of density near free-stream is required for high-speed flows.

REFERENCES

Durbin, P.A. 1996 On the k-3 stagnation point anomaly. *Int. J. Heat and Fluid Flow* **17**, 89–90.

Fluent, Inc. 2006 *Fluent 6.3 documentation*. Lebanon, New Hampshire.

Horstman, C. C. & Owen, F.K. 1975 Mean and fluctuating flow measurements of a fully-developed, non-adiabatic, hypersonic boundary layer. *J. Fluid Mech.* **70**, 393–413.

Lakshmipathy, S. 2008 Partially-averaged Navier-Stokes method for turbulence: fundamental validity and low-Reynolds number modification. PhD dissertation, Texas A&M University, College Station, Texas.

Moore, J. G. & Moore, J. 1999 Realizability in two-equation turbulence models. *AIAA Paper* 1999-3779.

Pirozzoli, S., Grasso, F. & Gatski, T.B. 2004 Direct numerical simulation and analysis of a spatially evolving supersonic turbulent boundary layer at M=2.25. *Physics of Fluids* **16**, 530–545.

Reynolds, W.C. 1987 Fundamentals of turbulence for turbulence modeling and simulation. *AGARD Rept.* 755.

Rotta, J.C. 1960 Turbulent boundary layers with heat transfer in compressible flow. *AGARD Rept.* 281.

Sarkar, S., Erlebacher, G., Hussaini, M.Y. & Kreiss, H.O. 1989 The analysis and modeling of dilatational terms in compressible turbulence. ICASE Report 89-79. Univ. Space Research Assoc., Hampton, Virginia.

Shih, T.-H., Liou, W. W. & Shabbir, A. 1995 A new $k-\epsilon$ eddy viscosity model for high reynolds number turbulent flows. *Computers Fluids* **24**, 227–238.

Sinha, K., Krishnan, M. & Candler, G.V. 2003 Modeling shock unsteadiness in shock/turbulence interaction. *Physics of Fluids* **15**, 2290–2297.

Tandra, D.S., Kaliazine, A., Cormack, D.E. & Tran, H.N. 2006 Numerical simulation of supersonic jet flow using a modified $k-\epsilon$ model. *Int. J. Comp. Fluid Dynamics* **20**, 19–27.

Thivet, F. 2002 Lessons learned from RANS simulations of shock-wave/boundary-layer interactions. *AIAA Paper* 2002-0583.

White, F.M. 2006 *Viscous fluid flow*, 5th edn. Boston, New York: McGraw-Hill, Inc.

Wilcox, D.C. 1992 Dilatation-dissipation corrections for advanced turbulence models. *AIAA Journal* **30**, 2639–2646.

Wilcox, D.C. 1994 *Turbulence modeling for CFD*, 2nd edn. La Canada, California: DCW Industries, Inc.

VITA

Sriram S. Arasanipalai obtained his B.Tech. degree in mechanical engineering from the Indian Institute of Technology, Madras, Chennai, India in July 2006. He began his master's work in the Department of Mechanical Engineering in August 2006. His areas of interests are fluid mechanics and heat transfer. Currently, he is working with CGGVeritas in Houston, Texas. His mailing address is 3225 Woodland Park Drive, Apt. 533, Houston, Texas, 77082 and his email address is sriram.sharan@gmail.com.

The typist for this thesis was Sriram S. Arasanipalai.